March 2002 • NREL/ SR-520-31984

Subcontractor Report

Characterization of Amorphous Silicon Thin Films and PV Devices

Final Technical Report January 1998 – October 2001

P.C. Taylor
University of Utah
Salt Lake City, Utah

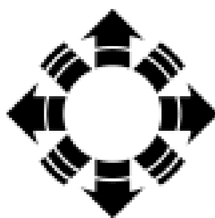

National Renewable Energy Laboratory

1617 Cole Boulevard
Golden, Colorado 80401-3393

NREL is a U.S. Department of Energy Laboratory
Operated by Midwest Research Institute • Battelle • Bechtel

Contract No. DE-AC36-99-GO10337

March 2002 • NREL/ SR-520-31984

Characterization of Amorphous Silicon Thin Films and PV Devices

Final Technical Report
January 1998 – October 2001

P.C. Taylor
University of Utah
Salt Lake City, Utah

NREL Technical Monitor: Bolko von Roedern

Prepared under Subcontract No. XAK-8-17619-13

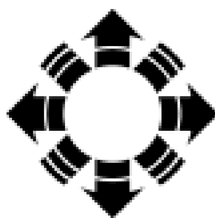

National Renewable Energy Laboratory

1617 Cole Boulevard
Golden, Colorado 80401-3393

NREL is a U.S. Department of Energy Laboratory
Operated by Midwest Research Institute • Battelle • Bechtel

Contract No. DE-AC36-99-GO10337

NOTICE

This report was prepared as an account of work sponsored by an agency of the United States government. Neither the United States government nor any agency thereof, nor any of their employees, makes any warranty, express or implied, or assumes any legal liability or responsibility for the accuracy, completeness, or usefulness of any information, apparatus, product, or process disclosed, or represents that its use would not infringe privately owned rights. Reference herein to any specific commercial product, process, or service by trade name, trademark, manufacturer, or otherwise does not necessarily constitute or imply its endorsement, recommendation, or favoring by the United States government or any agency thereof. The views and opinions of authors expressed herein do not necessarily state or reflect those of the United States government or any agency thereof.

Available electronically at http://www.osti.gov/bridge

Available for a processing fee to U.S. Department of Energy
and its contractors, in paper, from:
U.S. Department of Energy
Office of Scientific and Technical Information
P.O. Box 62
Oak Ridge, TN 37831-0062
phone: 865.576.8401
fax: 865.576.5728
email: reports@adonis.osti.gov

Available for sale to the public, in paper, from:
U.S. Department of Commerce
National Technical Information Service
5285 Port Royal Road
Springfield, VA 22161
phone: 800.553.6847
fax: 703.605.6900
email: orders@ntis.fedworld.gov
online ordering: http://www.ntis.gov/ordering.htm

Printed on paper containing at least 50% wastepaper, including 20% postconsumer waste

Table of Contents

1. Introduction 1

2. Second Harmonic Detection of ESR 3

3. Light-Induced Defects in a-SiS_x:H Alloys 7

4. Optically Induced Electron Spin Resonance in a-Ge:H 12

5. Low Temperature Kinetics of Band-Tail Carriers and Silicon Dangling Bonds 18

6. Direct Detection of Molecular Hydrogen by ^{1}H Nuclear Magnetic Resonance 33

7. Growth of Films and p-i-n Solar Cells 45

8. Conclusions 46

9. References 47

10. Publications 52

1. INTRODUCTION

Objectives

The major objectives of this subcontract are (1) to prepare new materials based on hydrogenated amorphous silicon (a-Si:H), (2) to characterize the important defects and impurities in the bulk and at surfaces and interfaces, (3) to identify metastabilities and to determine if the metastabilities that plague devices are "intrinsic" or "extrinsic," (4) to obtain a better understanding of how defects affect device performance.

Approaches

Two major approaches are utilized both (1) to improve the understanding of metastabilities in a-Si:H, alloys based on a-Si:H, microcrystalline alloys, and devices and (2) to develop schemes to mitigate the deleterious metastabilities in these materials and devices. First, novel alloys, such as those containing sulfur or selenium, are grown and characterized. Special emphasis is placed on understanding how impurities affect the electronic properties of such alloys and of devices based on such alloys. Second, a wide array of characterization techniques is employed to study the optical and electronic properties. The optical techniques include optical absorption as measured using photo-thermal deflection spectroscopy (PDS), photoluminescence (PL), PL excitation spectroscopy, optically detected or optically pumped electron spin resonance (ESR) and other spectroscopies using a wide range of optical sources. The major magnetic resonance technique is ESR. The transport techniques are photoconductivity (PC) and the constant photocurrent method (CPM).

Research Tasks

The subcontract is divided into two tasks. One task is the growth of doped and undoped a-Si:H and related alloys. At the start of this sub-contract the plasma assisted chemical vapor deposition (PECVD) system was up-graded to a three-chamber system capable of making state-of-the-art films and devices. This PECVD system has been making state-of-the-art films and p-i-n devices of moderate efficiency. Alloys with concentrations of group VI elements, such as sulfur [see publications 1-5] or selenium [see publications 6, 7], have been found to exhibit very inefficient, n-type doping. The photoluminescence (PL) spectra and photoluminescence excitation (PLE) spectra in a-Si:H alloyed with Se have been investigated [see publication 8].

A second task is the characterization of a-Si:H and related alloys and devices. We have used photoconductivity (PC) [see publication 9] and PL excitation spectroscopy (PLE) to probe defects which produce absorption below the gap in a-Si:H [see publication 10]. We have also used ESR [publications 11-13] and spin-dependent photo-induced absorption (PADMR) [see publication 14] to study defects in a-Si:H and related alloys. Second harmonic detection of optically induced ESR (LESR) has been employed to measure the universal decays of band-tail electrons and holes in a-Si:H [see publications 15 through 18]. LESR has been observed in a-Ge:H alloys [see publications 19 and 20]. Investigations of the production of silicon dangling bonds in a-Si:H at low temperatures have been performed [see publications 16 and 21]. In addition, the role of molecular hydrogen (H_2) has been investigated in samples of a-Si:H grown by the plasma enhanced chemical vapor deposition (PECVD) and hot wire CVD (HWCVD)

techniques [publications 22 through 25]. Finally, PL from Er^{3+} in partially crystalline a-Si:H has been measured [publications 26, 27], and the topography of microcrystalline Si:H samples has been observed in films made by MVSystems [publication 28]. A review of some of the earlier work performed under this sub-contract is also available [publication 29].

The most significant results of the three phases of the sub-contract are (1) the development of a second harmonic detection technique for ESR and optically excited ESR (LESR) in a-Si:H and related alloys, (2) the discovery of universal kinetics for the decay of optically excited electrons and holes in a-Si:H and related alloys at low temperatures, (3) the first detection of optically excited band tail electrons and holes in hydrogenated amorphous germanium (a-Ge:H), (4) the first electron spin resonance (ESR) study of the kinetics for the production of silicon dangling bonds in a-Si:H at low temperatures, and (5) the determination from ^{1}H NMR that there exists an order of magnitude more molecular hydrogen (H_2) in a-Si:H than previously measured.

2. SECOND HARMONIC DETECTION OF ESR

Electron spin resonance (ESR) and light-induced ESR (LESR) in a-Si:H have been studied for many years. In the dark there exists an ESR resonance at g = 2.0055 and a peak-to-peak linewidth of the usual derivative spectrum of ΔH_{pp} of about 7.5 G. This spectrum is attributed to a silicon dangling-bond defect. Below 40 K these dangling-bond defects are very difficult to observe because of a technical difficulty known as microwave-power saturation. For this reason we have perfected a "rapid passage" technique to increase the sensitivity of these measurements. To ;test this technique we have measured the LESR at about 40 K. In LESR two additional signals appear, a broad line at g = 2.01 with $\Delta H_{pp} \approx 20$ G and a narrow line at g = 2.004 with $\Delta H_{pp} \approx 6$ G. The broad line has been assigned to holes trapped in the valence-band tail and the narrow line to electrons trapped in the conduction-band tail. Prior to our recent results [1] there were no detailed kinetic measurements of the low-temperature LESR in a-Si:H. The reason that detailed measurements were not performed previously is simply that the ordinary derivative detection technique does not provide sufficient signal-to-noise ratios. However, using the second-harmonic technique the saturation of the LESR (and also of the dark ESR) signal with increasing microwave power is drastically reduced. With this technique we have measured the LESR lineshapes and kinetics over a wide range of excitation intensities.

Figure 1a shows a second-harmonic LESR spectrum measured at 40 K using 20 mW microwave power. At this microwave power the normal derivative signal would be greatly reduced due to saturation effects. As a comparison, the integral of a low-microwave-power (2 μW)., first-harmonic spectrum is shown in Fig. 1b. It is clear that the lineshapes ;of the two spectra are very similar, although certainly not identical. The smooth lines in Fig. 1 are fits with two Gaussian distributions [1].

The ratio of the broad line to the narrow line is larger in the second-harmonic spectrum. This phenomenon is caused by the different saturation behaviors of the broad and narrow lines in the two detection schemes. It is not easy to get an accurate measurement of the spin density using only the second-harmonic detection, but one can accurately measure spin densities using the second-harmonic detection scheme if the signals are tied to unsaturated measurements of the signal using the ordinary detection scheme. In this way one may measure dark ESR spin densities that are well below 10^{16} cm^{-3} at low temperatures provided that the samples are thick enough so that the ESR is not dominated by spins at surface states.

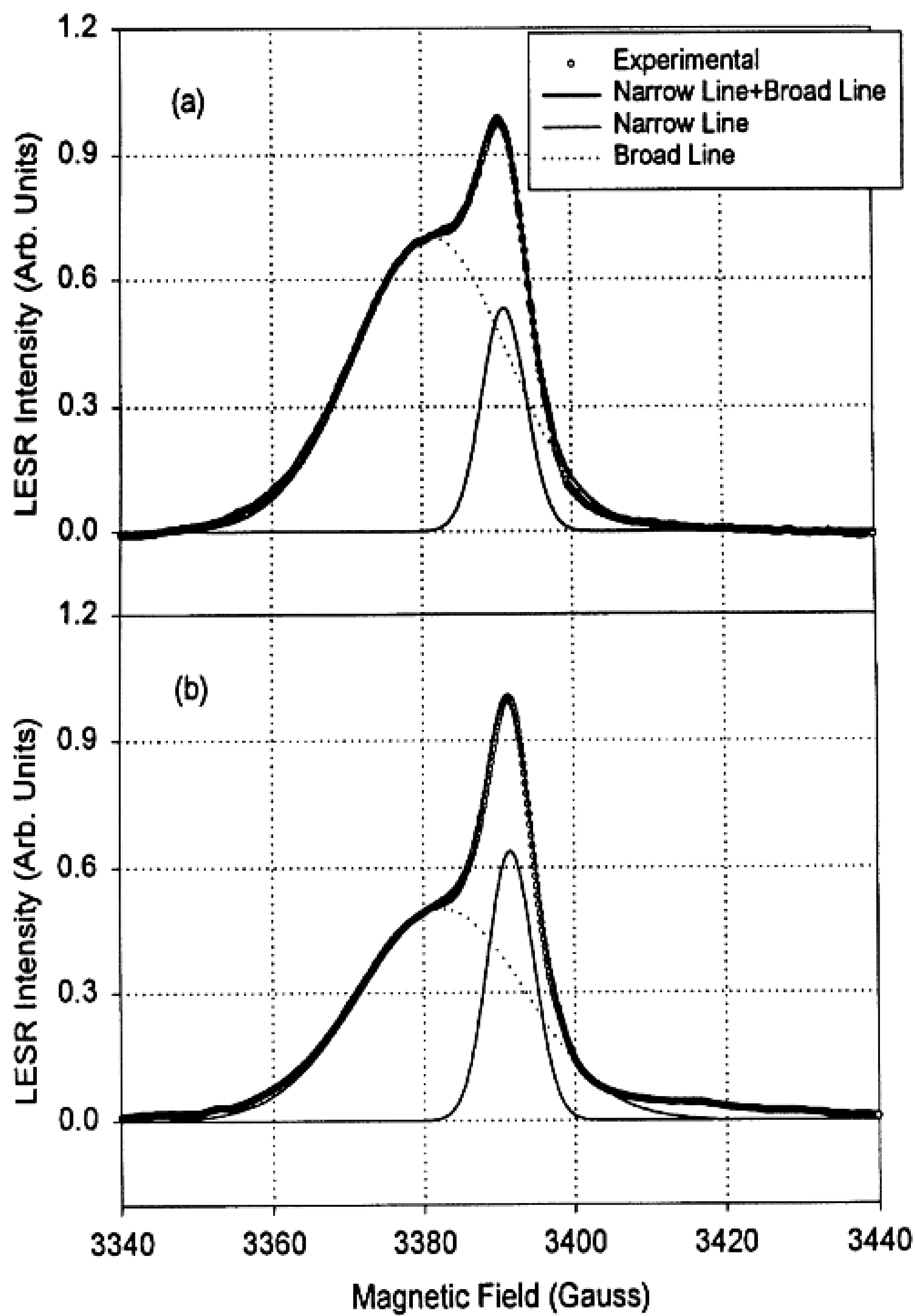

Fig 1. (a) LESR spectrum measured by second harmonic detection with 20 mW microwave power; (b) Integral of a first harmonic spectrum measured with 2μW microwave power. The smooth lines are fits with Gaussian distributions. Both spectra were measured at 40 K with 12 mW/cm2 excitation intensity.

Figure 2 shows that at 40 K the second-harmonic signal does not saturate appreciably with increasing microwave power even though the first-harmonic signal is very easily saturated. The magnitude of the second-harmonic signal grows roughly linearly with increasing microwave magnetic field (roughly as the square root of the microwave power). At low microwave fields the dependence is slightly super-linear while at high microwave fields the dependence becomes slightly sub-linear. This behavior is expected theoretically [2].

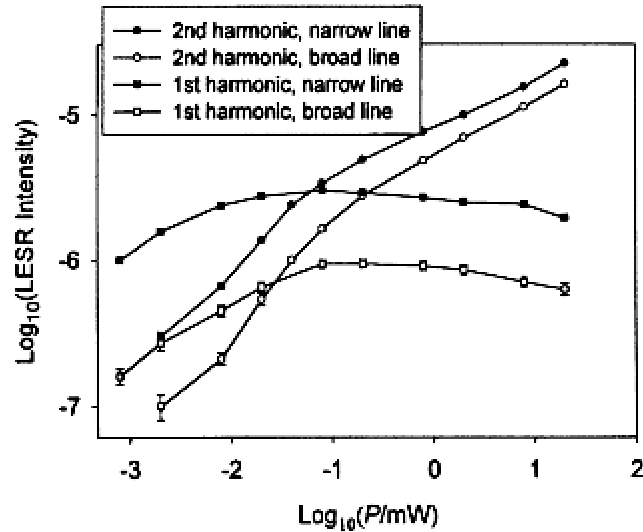

Fig. 2 LESR intensity versus microwave power (P). The first-harmonic data were measured using peak-topeak heights of the derivative spectra and the second-harmonic data were measured using peak heights of the absorption spectra from the base line.

The increase of the narrow line with increasing microwave power is slower than the increase of the broad line, a fact that leads to the relative suppression of the narrow line in Fig. 1a. Figure 2 also shows the extensive saturation of the first harmonic signal. It is clear from Fig. 2 that at 40 K the first harmonic signal is partially saturated even at the lowest attainable microwave powers. In addition, the saturation occurs much more easily for the narrow line than for the broad line. Since saturation is always a problem at this temperature, one may easily underestimate the intensity in the narrow line using the commonly employed first-harmonic-detection scheme. There is some evidence for such an underestimate in the literature [3].

Even though it is not central to the solution of problem of eliminating the metastabilities in a-Si:H films and PV devices, whether or not there exist significant numbers of charged defects in a-Si:H is an important question. From the defect pool model [4] it has been suggested that the density of charged dangling-bond defects is considerably greater than that of the neutral defects, even in device-quality a-Si:H. Some recent measurements also tend to confirm this suggestion [3, 5, 6, 7]. Some of these conclusions have been based on the ratio of the spin densities in the broad and narrow lines of the LESR. Although the detailed reasons are not clear, it is well known that the LESR measurements only measure a fraction of the light-induced carriers in the band tails. Fast geminate recombination and short spin-spin relaxation times are clearly two important reasons why no LESR is observed for carriers trapped in shallow band-tail states. Probably only deeply trapped carriers exhibit LESR because the localization lengths decrease with increasing trapping energy. Because we do not know what energy distinguishes whether

the trapped carriers yield a LESR signal, and furthermore we do not have any reason to assume that these energies are the same for trapped electrons and trapped holes, we may not expect that the spin density ;of the broad line must be equal to that of the narrow line, even in the absence of artifacts such as microwave saturation or of charged defects. Therefore, to postulate the existence of charged defects based solely on the LESR results is unfounded. In addition, subtle saturation effects, even in the second-harmonic-detection case, may also influence the accuracy of the decomposition into trapped electrons and trapped holes.

We have employed the second-harmonic detection scheme described above to measure the dark ESR spin densities in samples of a-Si:H made with and without hydrogen dilution as supplied by the group of C. R. Wronski at Penn State University. Samples were measured before and after light soaking for about 20 hours with approximately 300 mW/cm^2 of filtered white light from an ELH lamp. Spin densities were calibrated using a weak pitch standard and the usual first-harmonic (derivative of absorption) detection mode.

Table 1. ESR Spin Densities in Selected Samples from Penn State University

Sample No.	Thickness (μm)	N_s (as deposited) (cm^{-2})	N_s (annealed) (cm^{-2})	N_s (light soaked) (cm^{-2})	Remarks
LJ69	1.8	$1.9 \pm 0.5 \times 10^{12}$			No dilution
LJ70	1.35	$1.7 \pm 0.5 \times 10^{12}$	$1.7 \pm 0.5 \times 10^{12}$	$1.0 \pm 0.1 \times 10^{13}$	No dilution
LJ71	0.85	$1.1 \pm 0.5 \times 10^{12}$			No dilution
LJ82	0.85	$4.2 \pm 0.5 \times 10^{12}$	$4.2 \pm 0.5 \times 10^{12}$	$9.2 \pm 0.5 \times 10^{12}$	H_2 dilution

Because we obtained a set of samples of different thicknesses (see Table 1) for the case of no hydrogen dilution, we are able to extract both the surface and bulk spin densities unambiguously for these samples. The surface spin density for this set of three samples is 5×10^{11} cm^{-2}, and the bulk spin density as deposited is $1.0 \pm 0.5 \times 10^{16}$ cm^{-3}. The two samples that were light-soaked were annealed at 180 ° C for four hours in a nitrogen atmosphere before irradiation. As shown in Table 1, this annealing had no effect on the dark ESR spin densities. Because there was only a single sample in the hydrogen-diluted case, we cannot separate the surface and bulk contributions to the spin density unambiguously; however, the measured densities are large enough that we strongly suspect that they represent bulk spin densities. [The calculated surface spin densities are about an order of magnitude too large to be realistic.] If we assume that the spin densities for the hydrogen-diluted sample are entirely due to bulk spins, then the densities calculated from Table 1 are 5.6×10^{16} cm^{-3} and 1.1×10^{17} cm^{-3} for the as-deposited and light-soaked states, respectively.

These results show that hydrogen dilution does not significantly affect the optically induced production of neutral silicon dangling bonds even though there appears to be an improvement in the stability of cells made using the hydrogen-dilution process. Further experiments on both cells and individual layers are necessary to confirm this conclusion.

3. LIGHT INDUCED DEFECTS IN a-SiS_x:H ALLOYS

One approach to removing the deleterious metastabilities that are known loosely and collectively as the Staebler-Wronski effect is the addition of chalcogen elements (S and Se) into a-Si:H. This approach has resulted in a decrease of the degradation of conductivity and photoconductivity after light-soaking. Wang et al.[8] found a persistent photoconductivity (PPC) in a-SiS_x:H films, whose effect on both the conductivity and photoconductivity is opposite to the Staebler-Wronski effect. It is possible that the presence of the PPC effect may increase the stability of the materials and devices.

Recent studies have shown that the Staebler-Wronski effect and the PPC effect occur on different time scales during light-soaking and anneal at different temperatures in a-SiS_x:H and a-$SiSe_x$:H [9]. A similar phenomenon has also been observed in compensated a-Si:H samples doped with phosphine and diborane [10]. Although a model based on optically-induced activation of sulfur donors during light-soaking has been proposed [11], there is still only weak experimental evidence to support the model. Sulfur can be a double donor in crystal silicon, and the lowest donor level is relatively deep [12]. In addition sulfur donors can be passivated by hydrogen atoms. The situation is more complicated in the amorphous phase. First, the random network in amorphous silicon provides the possibility for chalcogen atoms to form two-fold-coordinated structures (the favorite coordination of chalcogen atoms), which is one factor that leads to the low efficiency of doping [13]. Second, the significant concentration of hydrogen in the materials may passivate the donors that are at substitutional sites.

Under the sub-contract we have measured the kinetics of generation and annealing of light-induced defects in a-SiS_x:H films and in undoped a-Si:H films. The defect density was measured by electron spin resonance (ESR) and light-induced ESR (LESR) techniques.

Figure 3 shows some examples of the ESR and LESR in a-SiS:H, where the feature labeled E′ center is from the quartz Dewar. The dark ESR spectrum is for a sample with 0.6 at. % sulfur after ten days light-soaking at 300 K. For this spectrum the dark spin density is 8×10^{16} cm^3. The g value of 2.0055 and the width of 7 to 8 G confirm that the dark ESR spectrum comes from silicon dangling bonds. The LESR spectra change with sulfur concentration. The broad line (observed at $g \approx 2.01$ for undoped a-Si:H) gradually disappears with increasing sulfur concentration as reported previously [14], and at the same time the LESR spin density increases [14]. The asymmetry of the LESR line for the sample with high sulfur concentration may be caused by an asymmetry in the g tensor or the spectrum may include more than one line. After comparison with the Se-alloyed sample, we believe that the LESR may come from defects (or traps) related to chalcogen atoms since the LESR spectra of a-$SiSe_x$:H are broader than those of a-SiS_x:H by a factor of 2 to 3. This increase in width from S to Se is expected if the width is due to g anisotropies that result from spin-orbit coupling. The spin-orbit coupling constant for atomic Se is approximately three times that for S.

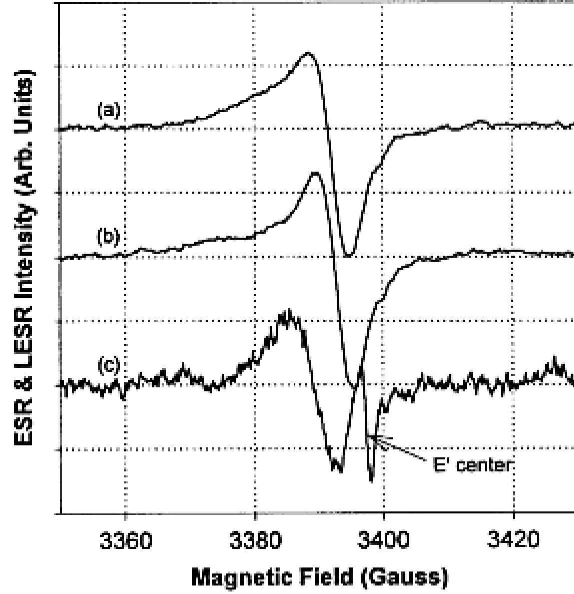

Fig. 3. ESR and LESR spectra of a-SiS_x:H. The LESR spectra [(a) and (b)] were measured at 40 K with 8 μW of microwave power. (a) 2 at. % of sulfur and (b) 0.6 at. % of sulfur. The ESR spectrum (c) was measured at room temperature with 20 μW of microwave power for the sample with 0.6 at. % of sulfur.

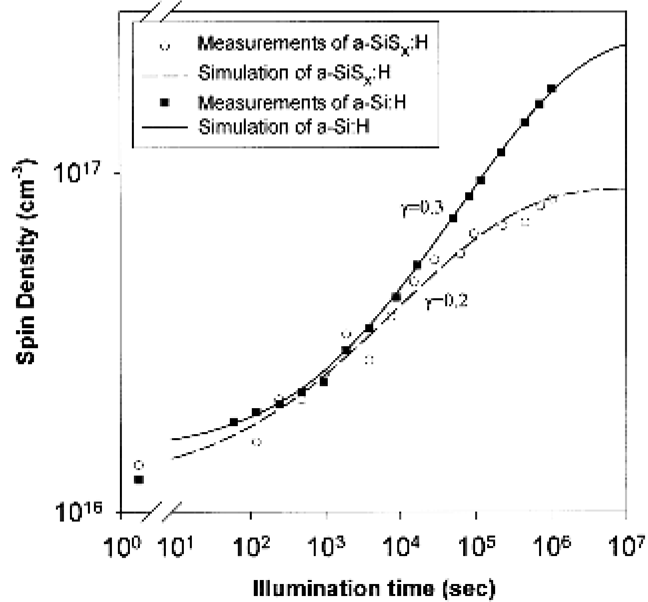

Fig. 4. Kinetics of light-induced defect generation for undoped a-Si:H and a-SiS_x:H ($x = 6 \times 10^{-3}$). The smooth lines are fits to the experimental data (symbols) with Eq. (1) with the parameters: $N_0 = 1.2 \times 10^{16}$ cm^{-3}, $N_S = 9 \times 10^{16}$ cm^{-3}, $\tau g = 8 \times 10^4$ s and $\beta = 0.38$ for a-SiS_x:H ($x = 6 \times 10^{-3}$); $N_0 = 1.5 \times 10^{16}$ cm^{-3}; $N_S = 2.5 \times 10^{17}$ cm^{-3}, $\tau_g = 8 \times 10^5$ s and $\beta = 0.45$ for a-Si:H

The generation kinetics of light-induced silicon dangling bonds in an a-SiS_x:H film (0.6 at. % S) and an undoped a-Si:H film are displayed in Fig. 4, where the symbols are experimental data and the lines are the fits to a stretched-exponential function [15],

$$N(t) = N_S - (N_S - N_0)\exp\left[-\left(\frac{t}{\tau_g}\right)^{\beta}\right] \quad , \qquad (1)$$

where, N_S is the saturated value, N_0 the initial value, τ_g the inducing time and β the dispersion coefficient. The parameters for the best fits to the experimental data appear in the caption of Fig. 4. Even though the initial values are roughly the same for the two samples, the saturated value is lower for the a-SiS_x:H sample ($x \approx 10^{-3}$) than for the undoped sample. Meanwhile, the dispersion coefficient, β is smaller for a-SiS_x:H than for undoped a-Si:H. Correspondingly, the approximate slope in the region of steepest ascent on a log-log plot (γ in Fig. 2) decreases from the usual value of 0.3 to approximately 0.2.

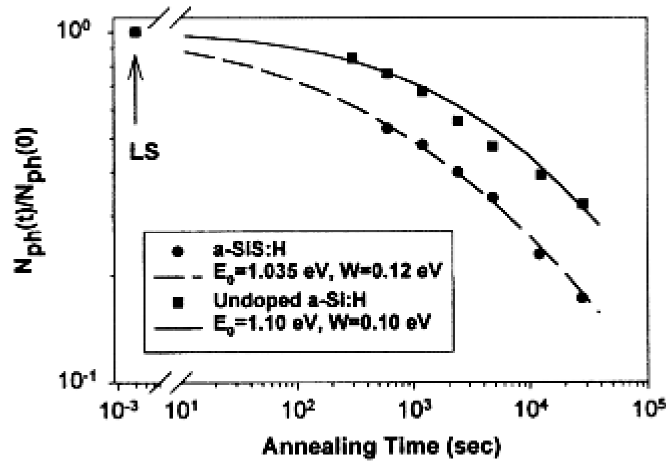

Fig. 5. Kinetics of light-induced defect annealing for undoped a-Si:H and a-SiS_x:H ($x = 6 \times 10^{-3}$). The smooth lines are fits to the experimental data with Eqs. (2) through (4) with the parameters: E_0 = 1.035 eV, W = 0.12 eV for a-SiS_x:H ($x = 6 \times 10^{-3}$); E_0 = 1.10 eV, W = 0.10 eV for a-Si:H.

Figure 5 shows the annealing kinetics of light-induced defects at 120°C. Clearly the light-induced defects are more easily annealed away in a-SiS_x:H than in a-Si:H. Based on the defect model of Hata and Wagner [16], there is a distribution of annealing activation energies (E_a). The defects with lower E_x anneal first, and the ones with higher E_a live longer. If the distribution of E_a is a Gaussian distribution, then

$$N(E_a) = \frac{N'_S}{\left(2\pi W^2\right)^{1/2}}\exp\left(\frac{\left(E_a - E_0\right)^2}{2W^2}\right) \quad , \qquad (2)$$

where N'_S is the initial value of the light-induced defects, E_0 the center and W the width of the distribution. The light-induced defect density remaining after annealing at a temperature T for a time t is

$$N(t) = \int_0^\infty N(E_a) \exp\left(-\frac{t}{\tau(E_a, T)} \right) dE_a \quad , \tag{3}$$

$$\tau(E_a, T) = \tau_0 \exp\left(\frac{E_a}{kT} \right) \quad , \tag{4}$$

The solid lines in Fig. 5 are the calculations using Eqs. (2) through (4). The parameters for the best fits to the experimental data are $E_0 = 1.035$ eV, $W = 0.12$ eV for a-SiS_x:H (x = 0.6 at. %) and $E_0 = 1.10$ eV, $W = 0.10$ eV for a-Si:H. Although the difference between the most probable activation energies is small for the two samples, this difference results in a significant change in annealing behaviors as indicated in Fig. 6. In this figure the curves show the distributions of E_a for the centers remaining after certain annealing times.

The incorporation of sulfur into amorphous silicon changes the structure of the material. Compared with undoped a-Si:H, the slower generation of light-induced defects is probably due to thermal annealing or to light-induced annealing during the light-soaking process. The kinetics governing the net generation of defects are a competition between generation and annealing. Therefore, if the generation rates are the same, the higher the annealing rate, the lower the saturated defect density. The experimental results confirm this scenario because the annealing activation energy is lower in a-SiS_x:H than in a-Si:H. Some recent studies show there are macroscopic changes occurring during light-soaking and annealing [17]. The low annealing activation energy in a-SiS_x:H may indicate that the network in this material is more flexible than in a-Si:H. This presumption is reasonable since the chalcogen atoms easily form two-fold-coordinated structures, such as occur in the standard chalcogenide glasses. Two-fold-coordinated structures may provide more flexibility to the underlying tetrahedral structure.

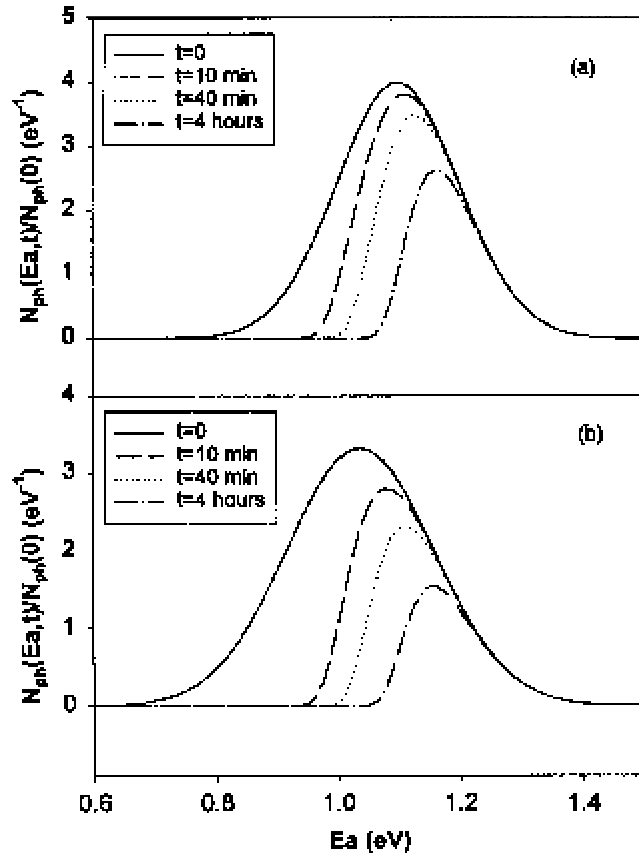

Fig. 6. Distribution of annealing activation energies with varied annealing times for (a) undoped a-Si:H and (b) a-SiS_x:H ($x = 6 \times 10^{-3}$).

The dark ESR spectrum at 300 K, both before and after light soaking, shows only the signature of silicon dangling bonds, which means the defects related to sulfur, if any, are not ESR active at this temperature. The increase of the low-temperature LESR with increasing sulfur concentration (the same trend happens to a-$SiSe_x$:H) suggests that the LESR signal may result from S-related defects, at least for the samples with high sulfur concentrations. One may speculate that either the S-related defects are in their charged states in the dark, as is the case in the chalcogenide glasses, or the S-related defects are passivated by the presence of hydrogen atoms, as can occur in crystalline silicon. Experimentally we did not find any change in the low-temperature LESR spectra or spin densities after prolonged light-soaking at 300 K. This fact indicates that there is no obvious increase in the S-related defects upon light soaking and confirms that any model for the sulfur-related LESR must involve the rearrangement of charge (or perhaps also of hydrogen atoms) at exiting defect sites rather than the creation of new defects.

4. OPTICALLY INDUCED ELECTRON SPIN RESONANCE IN a-Ge:H

Paramagnetic centers in amorphous silicon and germanium thin films were first identified by Brodsky and Title in 1969 by electron spin resonance (ESR) measurements [18]. The strength of the ESR signal is proportional to the number of paramagnetic centers, providing a powerful tool to probe the microstructure of these materials. The dominant ESR centers in hydrogenated amorphous silicon (a-Si:H) and hydrogenated amorphous germanium (a-Ge:H) are attributed, respectively to unpaired electrons at neutral silicon or germanium dangling bonds in the bulk of the films. Two additional paramagnetic centers have also been identified in phosphorous- and boron-doped a-Si:H [19,20] and a-Ge:H [21], and ascribed to localized electrons and holes in the conduction- and valence-band tails, respectively. Similar lines have been detected in a-Si:H by light-induced electron spin resonance (LESR)[19,20]. In spite of a number of attempts over the last 20 years [22,23], no similar LESR has been detected in a-Ge:H. In the last two quarters we have observed LESR in a-Ge:H, and we attribute the signals to holes and electrons trapped in the valence- and conduction-band tails, respectively. The observation of LESR in a-Ge:H allows the recombination kinetics and doping mechanisms in this amorphous semiconductor to be compared with those observed in a-Si:H and therefore allows potentially universal features to be identified.

The LESR derivative spectrum, as shown in Fig. 7a, resembles those obtained for a-Si:H [20] and is apparently also composed of two components, one narrow and one broad. In a-Si:H the narrow line, which peaks at higher field, has been attributed to electrons trapped in conduction band-tail states, while the broad line has been ascribed to holes in valence band-tail states. The LESR spectrum of Fig. 7a was fit assuming two paramagnetic sites. Because of limited information, the LESR powder-pattern lineshapes were calculated assuming the same anisotropy in the g-tensor as that which fits the dark ESR response due to Ge dangling bonds. The width introduced by the anisotropy is consistent with that expected by scaling the upper bounds for the anisotropy in the dark ESR and LESR observed in a-Si:H by the ratios of the spin-orbit coupling constants for Si and Ge (λ_{Ge}= 0.138 eV and λ_{Si} =0.019 eV [24]). This procedure amounts to assuming that the dangling bond, the electron trapped in a conduction-band-tail state, and the hole trapped in a valence-band-tail state are electronically similar for a-Si:H [25] and a-Ge:H. The two new LESR lines observed in a-Ge:H after light excitation are: 1) a broad resonance with a peak-to-peak width of ~60 gauss centered near g=2.03 and, 2) a narrow resonance with a width ~26 gauss centered at g=2.01. The two LESR lines saturate at different microwave power levels, which is an indication that they are due to two different ESR centers. In particular, the narrow line saturates at higher microwave power, which is different from the behavior observed previously in a-Si:H [26]

From the results of the computer simulation we find that the ratio between the density of paramagnetic spins due to holes and electrons, C_p/C_n, is about 1 ± 0.3. In a-Si:H this ratio depends on a number of conditions and is typically in the range 2 to 5 [25,26]. The origin of the deviation from a one-to-one ratio between the lines attributed to holes and electrons in a-Si:H has been a matter of some debate. This deviation has been attributed to spin pairing, to a change in the ratio of charged to neutral defect densities [26], or to certain artifacts of the ESR measurement technique [25]. In a-Ge:H it appears that none of these mechanisms is important.

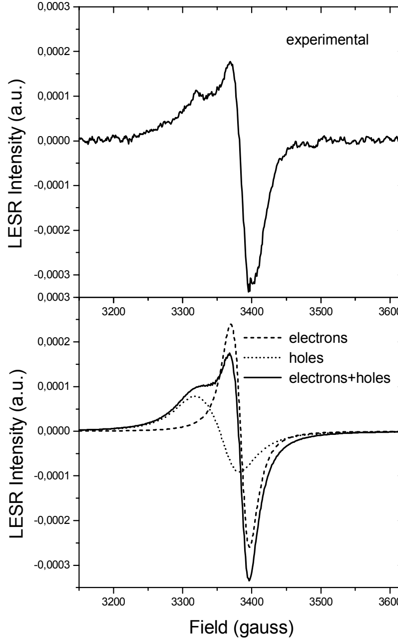

Fig. 7. (a) Light induced electron spin resonance of a-Ge:H, obtained by subtracting the signal in the dark from that under light excitation. (b) Fit to the experimental spectrum using two ESR centers.

Due to the high density of dangling bonds in the a-Ge:H (~$2x10^{17}$ cm^{-3} in the sample used in this study) compared to the density of the optically excited electrons and holes (~$2x10^{16}$ cm^{-3}), a small positive (or negative) LESR of the dangling bonds would cause a dramatic change in the hole-to-electron ratio. In a-Si:H the ratio between the LESR and dark ESR due to silicon dangling bonds is usually much greater than unity. Since C_p/C_n is near unity one can conclude that spin pairing and changes in the densities of neutral or charged defects are not important for the interpretation of the LESR in a-Ge:H. These results may prove useful for understanding the origin of the deviation in a-Si:H.

Information concerning the kinetics of the photo-generated carriers can be obtained through an analysis of the time dependence of the LESR. In Fig. 8 we show generation and decay curves of the LESR centered at 3400 gauss in a-Ge:H. At this magnetic field the LESR is mainly attributed to electrons in the conduction-band tail. As also occurs in a-Si:H, some photo-generated carriers are still present about 30 minutes after the light is turned off. The generation and decay of the broad line (measured at a fixed field of 3300 gauss, and attributed to holes), follow the same time dependencies as the generation and decay of the narrow line. A ratio of ~1 was obtained between both lines as a function of time. The solid curves in Fig. 8 are fits assuming a dispersive model for deeply trapped carriers. Details of the kinetic model, which was developed for a-Si:H, are available elsewhere [25,27]. In this model the recombination is assumed to be bimolecular. In a-Ge:H a dispersive parameter $\beta \sim 0.5$ was found for both generation and decay. Similar results were obtained for a-Si:H [25].

There are several reasons why LESR had not been observed in a-Ge:H after more than two decades of investigation. The main reason is the fairly large number of germanium dangling bonds, which normally lies in the 10^{18} to 10^{20} cm^{-3} range, and masks the observation of any LESR. For instance, even for the relatively high quality a-Ge:H studied here, with ~$2x10^{17}$ cm^{-3} dangling bonds, the density of photo-excited carriers is about one order of magnitude smaller, ~$2x10^{16}$ cm^{-3}. Second, the line width W is very large, due to the large spin-orbit coupling constant of germanium. Since the

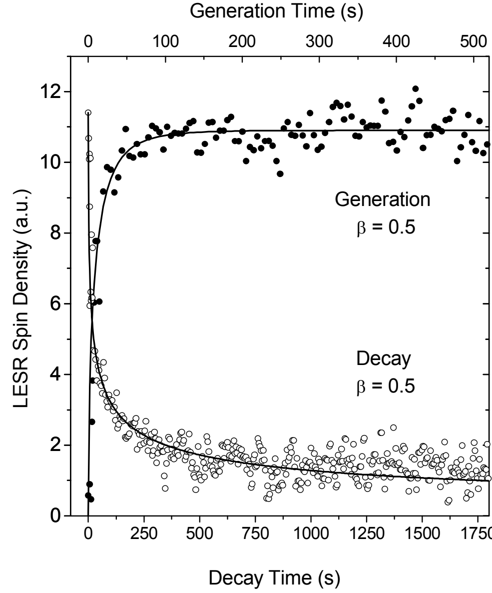

Fig. 8. Generation and decay of the LESR signal at 3400 gauss. At this magnetic field the signal is attributed mainly to electrons trapped in conduction-band tail. The data are averaged over four independent measurements, each performed without previous exposure to light.

intensity of the derivative signal goes approximately as W^{-2}, the signal is strongly reduced. For example, the measured peak intensity of the electron derivative line in a-Ge:H is roughly reduced to $(W_{Ge}/W_{Si})^{-2}$ ~ 10% of that of a-Si:H, for the same number of excited spins. Third, the LESR signal depends only weakly on the light intensity, $N \propto I^{0.27}$. The power was varied by more than four orders of magnitude, while the LESR intensity varied only by about one order of magnitude. Thus, using high power is not of much help for measuring LESR in a-Ge:H. Fourth, the absorption coefficient of a-Ge:H at ~2.0 eV, where most previous experiments were performed, is roughly one order of magnitude higher than the absorption coefficient near the band gap (E_{04} ~1.2 eV, E_{Tauc} ~1.1eV). The use of photon energies near the band gap allows the excitation of carriers throughout the bulk of the film. This condition was achieved using a Nd:YAG laser (1.17 eV).

The growth of the LESR signal is the result of the trapping of carriers in the band tail states when the film is under light exposure. This process takes a relatively long time, of the order of minutes, depending on the light intensity, as displayed in Fig. 9. The higher the laser power the faster the increase of the LESR signal and the higher the final steady state density of trapped electrons and holes. The solid line in Fig. 9 represents a fit using the phenomenological model developed by Yan et al. [25]

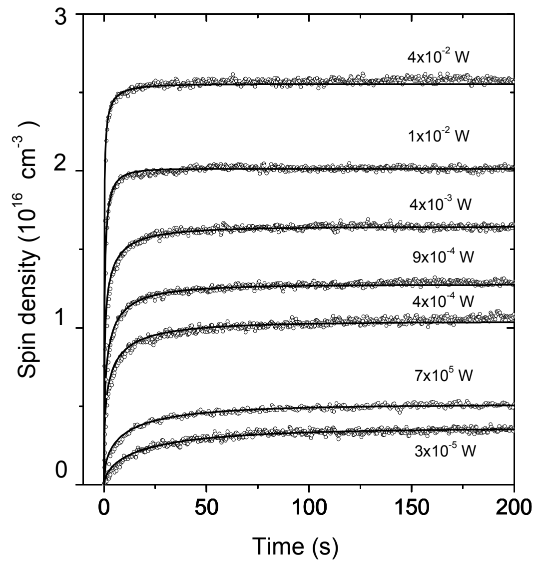

Figure 9. Time dependence of the growth of the light induced spin density as a function of laser power ($\propto$ light intensity) in a-Ge:H at 25 K

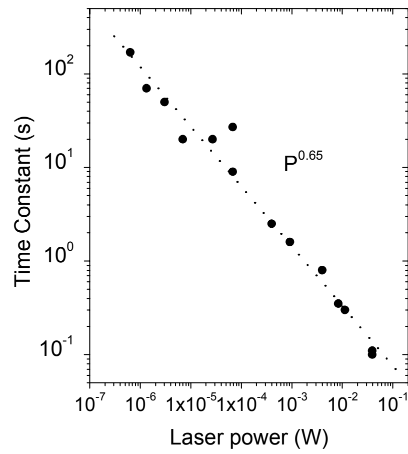

Figure 10. Characteristic time constant for growth of LESR as a function of laser power in a-Ge:H at 25 K. The solid line is a linear regression fit to the data.

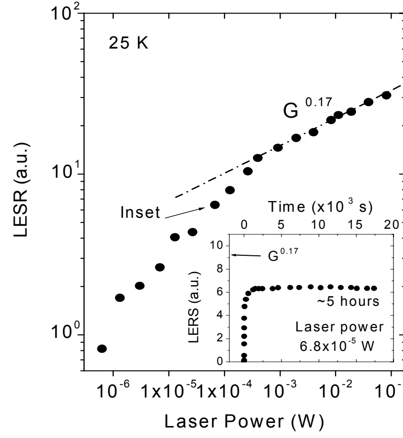

Figure 11. Saturated spin density as a function of laser power in a-Ge:H at 25 K. The inset represents the time dependence of the growth for a laser power of 6.8 $x10^{-5}$ W (see indication on the main figure). The saturated spin density obtained from this curve does not match the $G^{0.17}$ power law regime observed for higher laser powers.

considering dispersive recombination of the electrons and holes through distant pair recombination. The characteristic time constant for the growth, obtained by that model, is displayed in Fig. 10. The data show that the time constant follows a power law function with an exponent of 0.65 over a range of about 5 orders of magnitude.

Figure 11 displays the saturated density of trapped electrons and holes as a function of the light intensity [See Fig. 9]. This figure shows that the final LESR has two regions of dependence on the light intensity. At high light intensity the LESR follows a power law function with an exponent of 0.17.

The solid curves in Fig. 9 are fits assuming a dispersive model (developed for a-Si:H [25]) for deeply trapped carriers. In this model the recombination is assumed to be bimolecular. A dispersive parameter $\beta \sim 0.5 \pm 0.2$ was obtained for the majority of the curves in Fig. 9 as well as for all other curves measured with laser power in the 10^{-6} W to 10^{-1} W range. These results suggest a bimolecular recombination process for the photo-generated paramagnetic carriers over the range of laser powers displayed in Figures 9 to 11, which comprise about 5 orders of magnitude.

Figure 10 shows that the characteristic time constant, which is related to the recombination lifetime, is proportional to $G^{-0.65}$. Using computer simulations, Levin et al. [28] found that the mean radiative lifetimes are proportional to $G^{-0.84}$, which is very close to the results shown in Fig. 10. Yan et al. [27] also reported time constants proportional to $G^{-0.7}$, in high quality PECVD a-Si:H, which is also very close to our result as well as to the predicted value proposed by Levin et al. [28].

As shown in Fig. 11, the saturated spin densities for high light intensities are proportional to G^{γ}, where $\gamma \sim 0.17$. The range of light intensities employed is approximately three orders of magnitude. Boulitrop and Dunstan [29] reported γ values for a-Si:H in the range of 0.17 to 0.29 depending on the temperature and on the sample. More recently, Yan et al.[27] also found a value of γ for a-Si:H of 0.24 using a second-harmonic technique for the detection of the ESR. All these experimental results for a-Ge:H and a-Si:H films are very close to that theoretically found by Levin et. al. [28], who predicted a power law dependence with $\gamma \sim 0.16$ due to bimolecular recombination of the photo-generated carriers in amorphous semiconductors. This model considers the probability functions for both geminate and distant-pair recombination processes as a function of time and light intensity. Our results for a-Ge:H, as well as the data reported for a-Si:H, can be explained by this model in which bimolecular recombination dominates over the range of generation rates covered in these investigations.

The light intensity dependence of the saturated spin density, as shown in Fig. 11, is different for low light intensities (laser power smaller than $\sim 10^{-3}$ W). A similar behavior has also been observed in a-Si:H by Yan et al. [25] and attributed to the long times necessary to achieve saturation at low light intensities. These authors observed that the saturated spin densities in a-Si:H may take hours or days to reach the equilibrium values at low light excitation. However, the behavior in a-Ge:H is different. As shown in the inset to Fig. 11, the saturated LESR signal for a laser power of 6.8×10^{-3} W is smaller than the expected value. [See the arrow on the inset or the extrapolated line of the $G^{0.17}$ curve on the main figure.] We observe no tendency of the LESR to increase after 5 hours of measurement, which is a time long enough to disclose any tendency for saturation at this particular laser power. Thus, there must be other reasons for this change in the light intensity dependence for the saturated spin density in a-Ge:H. Additional investigation is required to clarify this issue.

5. LOW TEMPERATURE KINETICS OF BAND-TAIL CARRIERS AND SILICON DANGLING BONDS

The most common metastability in the electronic properties of hydrogenated amorphous silicon (a-Si:H) is the Staebler-Wronski (S-W) effect [30], which is a decrease in both the photo- and dark conductivities after excitation with light of energy close to the optical bandgap. Most models that attempt to explain this effect attribute the decreases in conductivity to a metastable increase in the density of silicon dangling bonds. For this reason it is important to understand the kinetics for the production of silicon dangling bonds. Photoconductivity experiments [31,32] have recently shown that the S-W effect is only weakly dependent on temperature between 4 K and 300 K. To explain this very weak temperature dependence a photo-enhanced diffusion process for hydrogen in a-Si:H has been proposed [33]. In the first two quarters of Phase II we have shown that the production of silicon dangling bonds, as measured by electron spin resonance (ESR), is much less efficient at 65 K than at 300 K and that the ESR measurements below about 100 K are complicated by the presence of long-lived, optically excited carriers trapped in localized band-tail states. At temperatures below about 100 K, previous measurements have shown that the lifetimes of optically excited carriers vary by several orders of magnitude [34,35]. Some carriers recombine rapidly (<1ms) [34], however, a subset of photoexcited carriers can have lifetimes in excess of several hours [35]. Some of these long-lived carriers can be induced to recombine (i.e., the densities can be bleached) by irradiation of the sample with low energy, infrared light. Presumably, the infrared light re-excites the trapped band-tail carriers into extended states, and therefore this light promotes diffusion and recombination of electrons and holes. This infrared bleaching or quenching mechanism is inferred from infrared light induced changes in photoluminescence (PL) [36], light induced ESR (LESR) [36], and photoconductivity (PC) [31,37,38]. However, although infrared quenching is known and has been frequently applied, little is known about its effectiveness in removing all long-lived, band-tail carriers as measured by LESR. Such measurements are crucial because the long-lived carrier densities can easily exceed the density of the silicon dangling bonds [39,40]. It is very difficult to distinguish the dangling bonds from the long-lived electrons trapped in conduction band-tail states by ESR measurements. The ESR response attributed to dangling bonds occurs at a g-value of approximately 2.0055, while the signals attributed to long-lived band-tail electrons and holes occur at g-values of approximately 2.004 and 2.01, respectively. Since the line widths for all three resonances are several Gauss, it is difficult to resolve these three resonances, especially the signals due to dangling bonds and band-tail electrons.

We first examine the kinetics and efficiency of infrared bleaching of long-lived photoexcited carriers. We set the magnetic field to the resonance field (approximately 3390 G) and monitored the peak of the resonance over time. The sample was cooled down in the dark. At t = 0 the ESR signal is solely due to the dark spin density and the concentration of long-lived, photoexcited carriers is zero, as shown in Fig. 12. First, we illuminate the sample for approximately 20 minutes with low intensity light. As shown in Fig. 12, for this illumination intensity, the LESR spin density initially rises rapidly and is followed by a slow component that increases for several hours at the light intensities employed in these experiments. After about 20 minutes of illumination we turn off the excitation and keep the sample in the dark. The sharp features in the spectrum between about 10 and 25 minutes are artifacts due to thermal instabilities during the measurement.

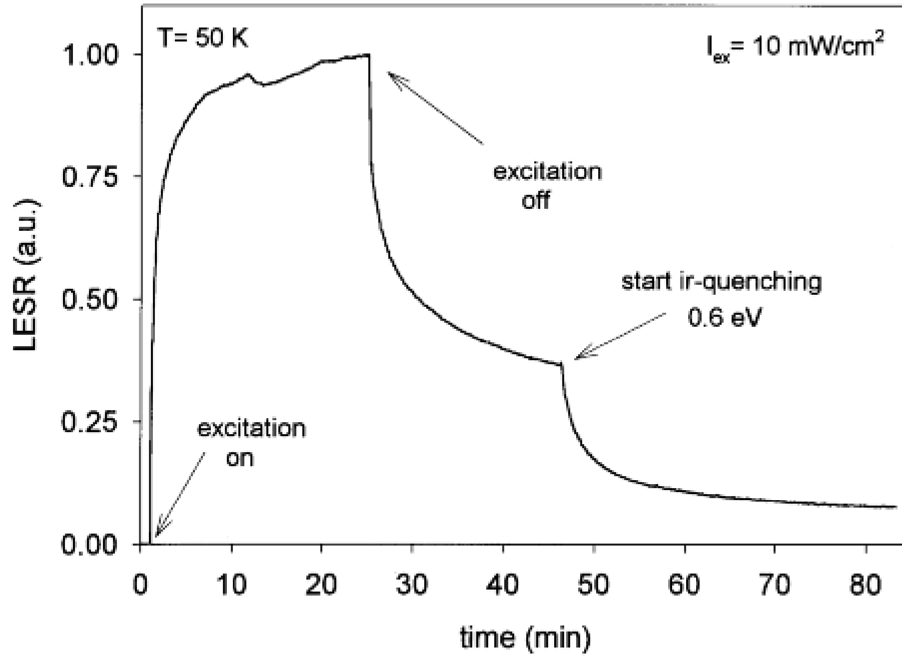

Fig. 12. Infrared quenching of residual LESR. The data up to approximately 45 min show the rise and decay of the LESR signal after the excitation source has been turned on and off, respectively. Infrared quenching is initiated after approximately 45 min with an infrared cut-off energy of 0.6 eV.

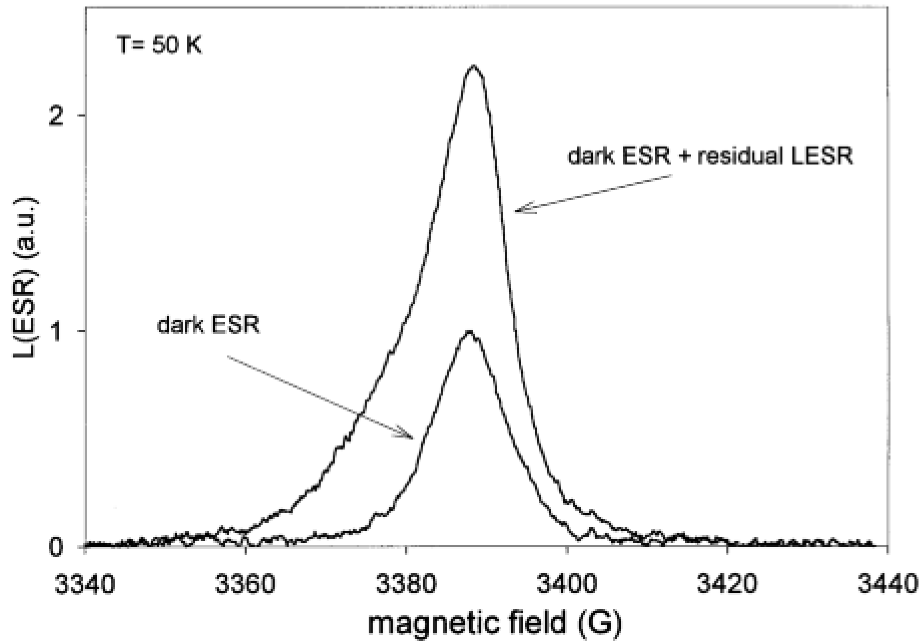

Fig. 13. ESR signal measured at t=0 min and t=85 min in Fig. 1. The dark ESR signal was taken immediately after cooling the sample down in the dark and is entirely due to silicon dangling bonds. The spin increase observed in the signal taken at 85 min over the dark ESR signal indicates a significant residual LESR carrier concentration that is not quenched by the ir-light.

After an initial rapid recombination of short-lived carriers, a very slow decay of the ESR signal continues due to long-lived carriers. This residual LESR signal remains even after several hours. We then initialize the photo quenching with low energy infrared light using a 0.6 eV high-energy cut-off filter. After about 45 min of ir-quenching, the residual LESR spin density is greatly reduced; however, a significant fraction of long-lived carriers remains. This situation is more clearly demonstrated in Fig. 13, which shows the ESR spectra taken immediately after the sample was cooled down in the dark, i.e., at t = 0 in Fig. 3, and immediately after the quenching, i.e., at t = 85 min. Clearly, the ESR signal taken after 45 min of ir-quenching (t = 85 min in Fig. 12) shows a significant increase over the dark ESR signal, indicating a residual LESR spin density that is not affected by the ir-quenching light. We performed several photo excitation-and-quenching cycles as shown in Fig. 12 with quenching energies that were cut off at different energies. We find that photo quenching of long-lived carriers becomes observable for photo quenching energies above about 0.35 eV, indicating that the most shallowly trapped, long-lived carriers (presumably the electrons) are trapped about 0.35 eV below the band edges. However, under all quenching light energies we find that a significant fraction of deeply trapped carriers is unaffected by the photo quenching. Light of approximately 1 eV either induces LESR or bleaches existing LESR, depending on the preexisting density of long-lived carriers.

Next, we examine the kinetics of the light induced production of silicon dangling bonds between 65 K and 340 K. From the measurements just described at low excitation intensities, we know that infrared quenching does not remove all the long-lived carriers. Therefore, to assure that the ESR signal is only due to dangling bonds, we annealed the sample for several minutes at 250 K before every low temperature ESR measurement at the irradiation temperature. Figure 14 shows two representative growth curves of silicon dangling bonds produced at 65 K and 340 K. Note the linear scales. After a total of 600 min of illumination the sample irradiated at 340 K shows a density that is about a factor of five greater than the sample irradiated at 65 K. Although the illumination time was not long enough, the upper curve seems to flatten at long times. This curve also is consistent with the commonly found sublinear dependence of the degradation on illumination time [41]. At 65 K a dependence on illumination time that is closer to linear is found.

Figure 15 shows the light induced dangling bond densities after 10 h of illumination at four temperatures between 65 and 340 K. It follows from Fig. 15 that the production rate of silicon dangling bonds decreases with decreasing temperature and drops by about a factor of five between 300 K and 65 K. If this process is assumed to be thermally activated, then the activation energy is approximately 0.01 eV. Recent measurements down to temperatures as low as 10 K have shown that the process is not truly activated, but rather saturates at the lowest temperatures.

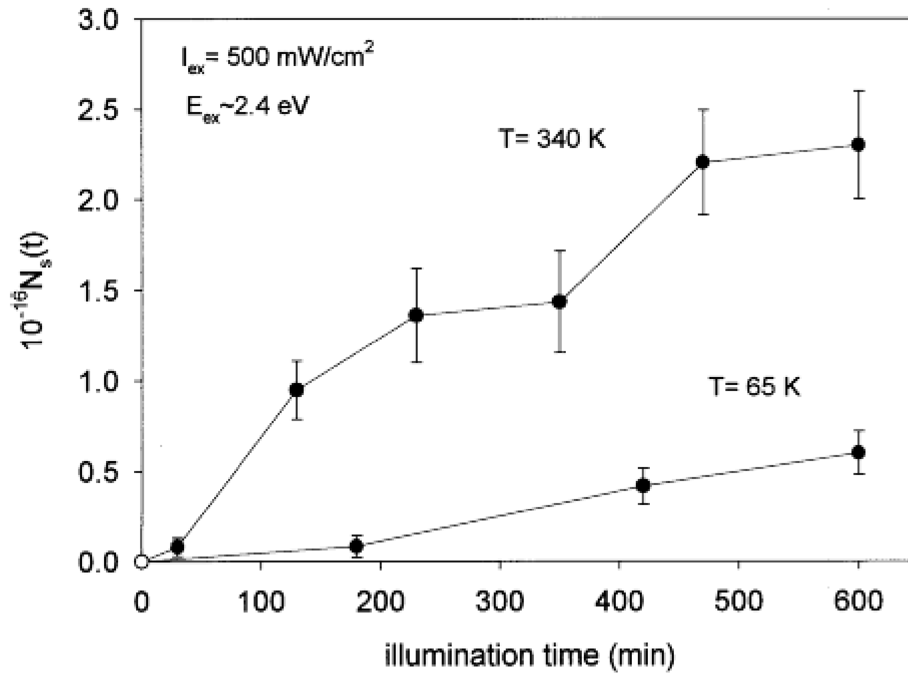

Fig. 14. Light induced silicon dangling bond production at 65 K and 340 K. ESR measurements were performed at the illumination temperature. At 65 K the sample was annealed at 250 K before each measurement.

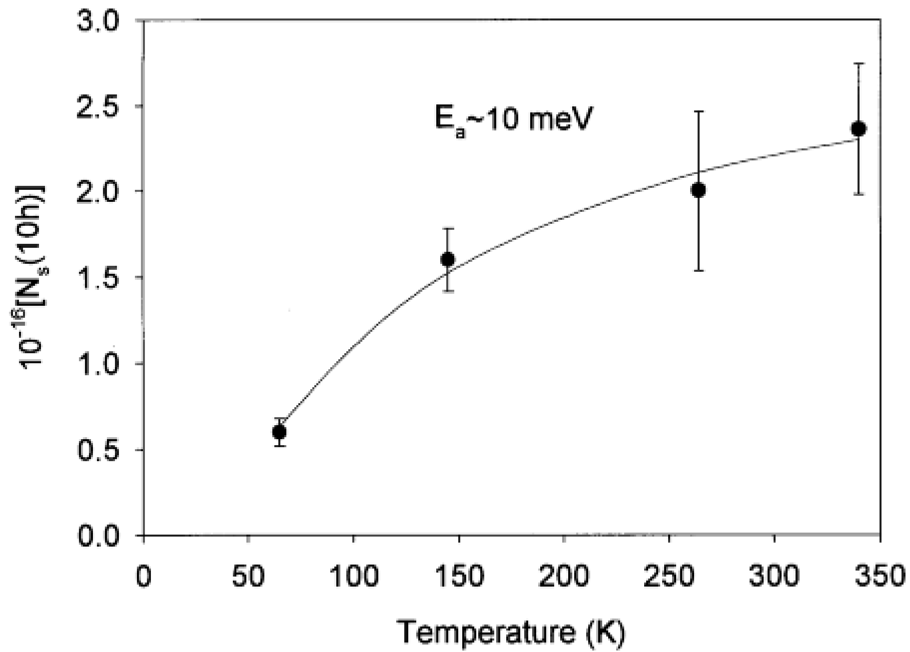

Fig. 15. Light induced increase in spin density $N_s(t)$ after t=10 h of illumination at four temperatures. If a thermally activated process is assumed, an activation energy of approximately 10 meV is found, as indicated by the solid line.

For the most recent measurements, we have used an a-Si:H sample that consisted of a stack of four a-Si:H films on quartz substrates with a spin density of about 5 x 10^{15} cm^{-3} including the surface spin density. The sample was mounted inside an ESR cavity equipped with openings to irradiate the sample inside the cavity. All experiments were performed on a standard ESR spectrometer (Bruker, Model 200D-SRC) at X-band. We investigated the ESR spin density by employing a second harmonic technique, i.e., by detecting the ESR signal at twice the magnetic field modulation frequency, which was set to 50 kHz. Except where otherwise stated, all ESR measurements were performed at about 50 K. For all degradation measurements a Xe arc lamp was employed. The light passed through a 580 nm long pass filter and had an intensity of approximately 100 mW/cm^2 at the sample. In every degradation measurement the sample was irradiated for 10 h. Annealing of the sample at temperatures, T, below 300 K took place inside the cavity by reduction of the He cooling gas flow. For annealing at T > 300 K the sample was removed from the cavity and heated for 30 min in a nitrogen atmosphere at about T = 200°C (470 K). All low temperature degradation measurements were immediately followed by a room temperature degradation, and all increases in spin densities were measured relative to the subsequent room temperature degradation. After 10 h of illumination the spin density increased by about 150% relative to the spin density of the as-deposited sample.

As described above, at temperatures below approximately 300 K the production of silicon dangling bonds depends on the temperature and that the production below approximately 100 K is at most half as efficient as at 300 K. In addition, the dangling bonds produced by up to 10 hours of irradiation below 100 K are unstable and anneal essentially completely at 300 K. The existing kinetic models that attempt to explain the S-W effect are not robust enough to explain this complex behavior. Here we suggest that there exists a two-step process whereby silicon dangling bonds can be produced essentially independently of the temperature, presumably mediated by optically excited carrier recombination, followed by hydrogen migration, which has a temperature-dependent component.

It is well known [42] that below about 150 K a subset of the photoexcited carriers can live for very long times, some of which easily exceed several hours. These carriers tend to swamp the signal from the silicon dangling bonds that are created at low temperatures (S-W effect). Some of these long-lived carriers can be induced to recombine (the densities can be bleached) by irradiation of the sample with low energy, infrared light. The assumption is that the lower energy infrared light re-excites the carriers trapped in the band tails and therefore promotes diffusion and recombination of electrons and holes. This mechanism has been inferred from changes induced by infrared light in photoluminescence (PL) [43], LESR [43], and photoconductivity (PC) [44,45,46]. Because PL and PC provide no microscopic information on the defects, and the standard detection of LESR is not sensitive enough to study the bleaching kinetics in any detail, the connections of these experiments with specific models have necessarily involved considerable conjecture. Our LESR results provide direct information on both the microscopic origins of the optically induced defects and the kinetics for their production and decay. In particular, although previous PC experiments [46,47,48] suggested that infrared light completely removed the band-tail carriers at low temperatures, our results show that a significant fraction of the long lived carriers is not affected by the quenching light on a laboratory time scale ($t<10^4$ s).

As mentioned above, detailed kinetic experiments using electron spin resonance (ESR) and light-induced ESR (LESR) at low temperatures are difficult due to saturation of the LESR signal as a result of long spin-lattice relaxation times. To solve this problem, we [27,49] have employed a second-harmonic detection technique that effectively eliminates this difficulty and allows for detailed kinetic experiments to be performed, even for small ESR spin densities. The improvement in effective signal-to-noise ratio can be several orders of magnitude at low temperatures. Whereas the standard detection of ESR results in a signal proportional to the derivative of the absorption, the second harmonic detection results in a line shape that roughly approximates the resonant absorption component. Details are available elsewhere [27,49].

Because the LESR signals due to electrons and holes trapped in localized band-tail states compete with the signal ascribed to silicon dangling bonds, we have examined the kinetics and efficiencies for infrared and thermal bleaching of the LESR signals attributed to band-tail electrons and holes. The two ESR responses attributed to band-tail electrons and holes occur at g-values of approximately 2.004 and 2.01, respectively, while the signal attributed to silicon dangling bonds occurs at approximately 2.0055. Because the line widths for all three resonances are several Gauss, the ESR responses due to band-tail electrons and silicon dangling bonds are difficult to resolve experimentally.

The LESR signal rapidly increases after the light is switched on. This rapid increase is followed by a slow increase that is still observable after several hours. Similarly, after the cessation of irradiation a rapid decay of the LESR signal is followed by a long tail that is still detectable after many hours in the dark. We examine the accumulation kinetics of these very long lived band tail carriers by the following measurement. Initially we cool down the sample in the dark and perform an ESR measurement (lowest curve in Fig. 16). We then go several times through the following inducing and bleaching cycle: We irradiate the sample for a certain amount of time that approximately doubled from 30 s to 60 min in every cycle. To emphasize the accumulation of long-lived, band-tail carriers, we employ 0.5 eV light for three minutes after every excitation to bleach the short-lived, shallowly trapped carriers. This bleaching procedure is very similar to that used in previous photoconductivity experiments. We do not find significant differences in the residual ESR spin densities after quenching with 0.5 eV or 0.6 eV light. After ir-quenching we keep the sample in the dark for approximately 10 minutes to establish an approximate equilibrium LESR density (on a time scale of minutes). By following this procedure we minimize the influence of any thermal relaxation during the subsequent measurement of the remaining LESR signals. In any case, small thermal decays will tend to affect all measurements in a similar fashion. Figure 16 shows the accumulation of band-tail carriers after successive irradiation and bleaching cycles. [The small feature just below 3400 G is an artifact and is due to E' centers [50] on the quartz substrates or in the quartz insert Dewar.] As shown in the inset to Fig. 16, the more stable band-tail carriers grow approximately as a power law in time, t, as $t^{1/3}$ until saturation. This dependence on time is often observed for the creation of silicon dangling bonds at room temperature [41], but in the present case the signal is exclusively due to electrons and holes that are deeply trapped in localized, band-tail states. This conclusion follows unambiguously from the ESR line shape that clearly shows a shoulder on the low field side, which is ascribed to holes trapped in valence band-tail states. A similar dependence on time of the increase in sub-band-gap absorption as measured by photoconductivity has been observed at low temperatures but in this case the increase was attributed to the production of defects contributing to the S-W-effect [49,51,52]. The most deeply trapped carriers in the conduction and valence band tails are very difficult to remove

optically. As the densities of trapped carriers get smaller, the probability that optical excitation will result in recombination is reduced relative to the probability for re-trapping.

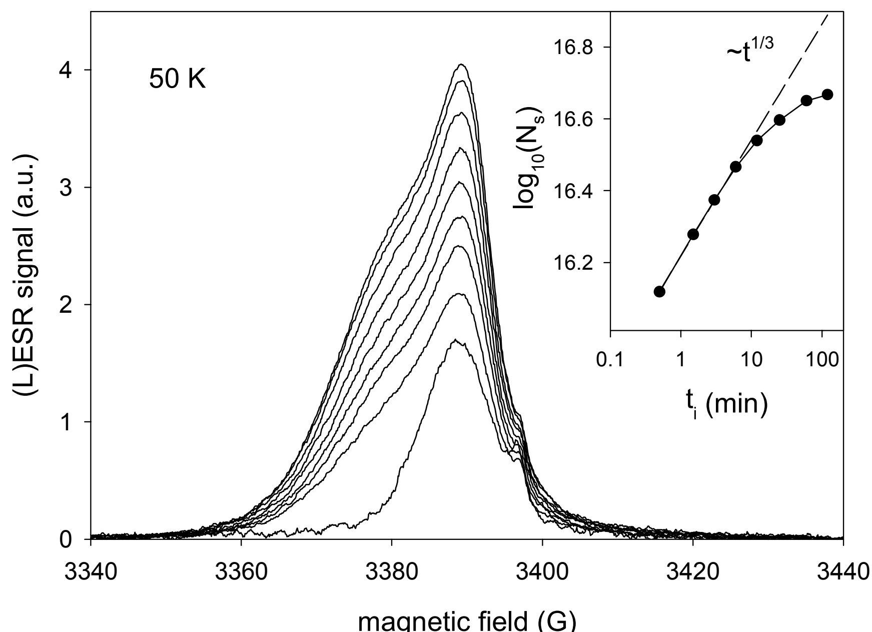

Figure 16. Accumulation of long lived spin carriers. Between two consecutive ESR measurements the sample was illuminated, exposed to 0.5 eV light for 3 min, and kept for 10 min in the dark. The abscissa shows the total illumination time. The smallest spectrum shows the dark ESR due to silicon dangling bonds. Inset: Increase of long-lived carriers relative to the dark ESR signal.

Now that we understand the influence of the optically excited band tail carriers on our measurements, we next examine the kinetics for the production of silicon dangling bonds at temperatures between 25 K and 300 K. Because this effect is very inefficient, even at 300 K, much greater light intensities were employed for these experiments. Preliminary results were shown above. Figure 17 shows an improved version of the increase in silicon dangling bond densities after 10 h of illumination with a xenon lamp (approximately 0.5 W/cm^2 at the sample) at five temperatures between 25 and 300 K. After each optical excitation at low temperature, ESR measurements were performed after ir-quenching and after annealing at 120 K, 220 K, and 300 K. Except for irradiations performed below 40 K, all ESR measurements were performed at 40 K to eliminate the influence of temperature on the ESR intensity. All low temperature degradation experiments were followed by a room temperature degradation with sample annealing in between. In Fig. 17 the degradation is presented relative to the room temperature degradation. Within the error bars the number of light-induced spins at $T< 100$ K as measured after ir quenching and annealing at 120 K are very similar, and so only the light-induced spin densities after 120 K annealing are shown in Fig. 17. The inset of Fig. 17 shows the relative degradation at low temperatures (squares) compared to room temperature for a different sample, for which laser excitation was employed. The ESR measurements were performed at the degradation temperature after annealing at 250 K. These data are compared to the data set of Fig. 17, where the annealing temperature was about 220 K (circles) and the LESR measurements were performed at 40 K. Only small differences that we ascribe to systematic errors are observable, indicating that the choice of our sample and the specific experimental procedure does not dramatically influence the results.

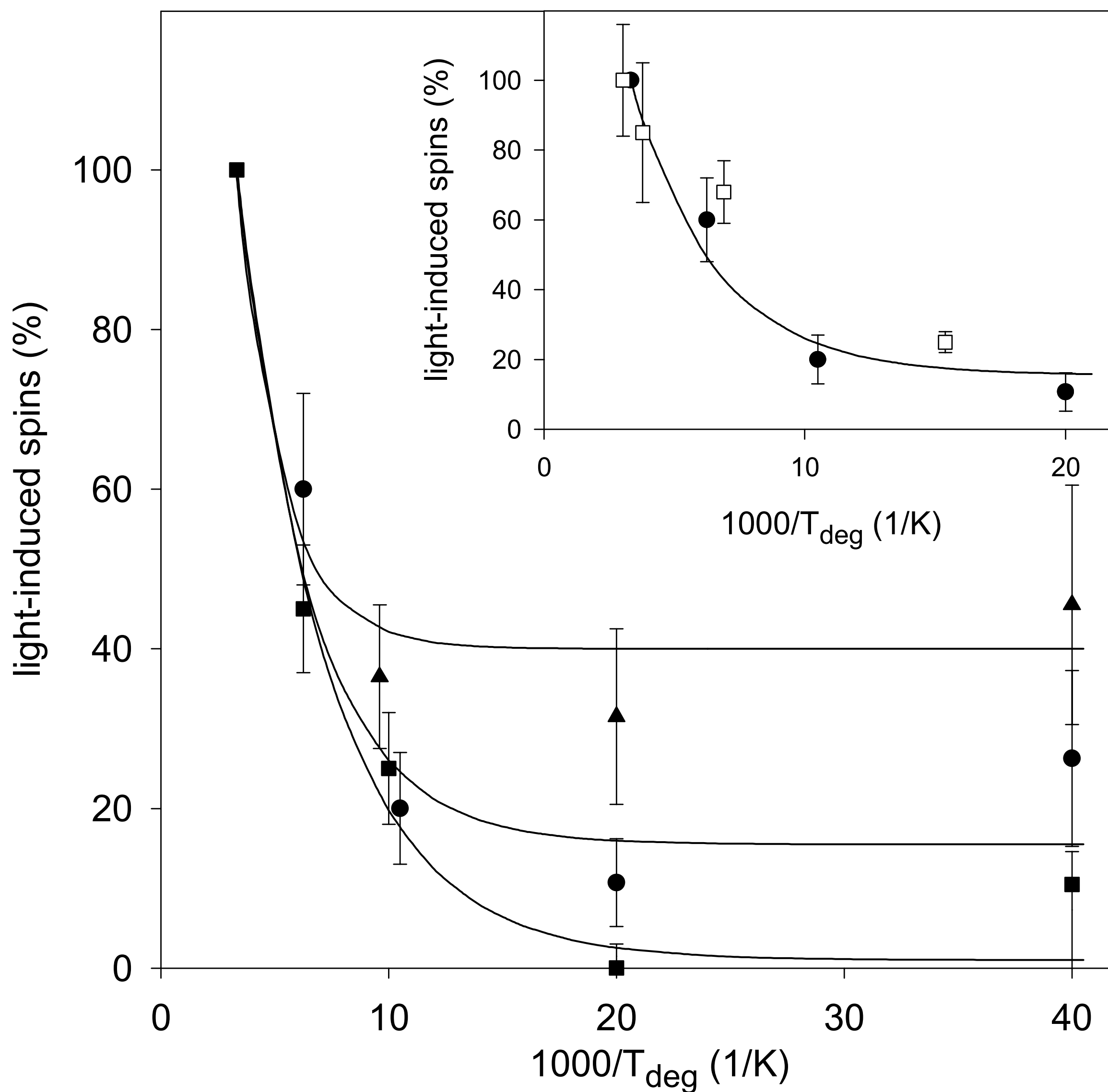

Figure 17. Light-induced increase in spin density after 10 h of illumination. After every illumination period the ESR spin density was measured after ir-quenching and annealing at 120 K (triangles), 220 K (circles) and 300 K (squares). All ESR data were obtained at 40 K and the data at 100 K are shifted for clarity. The inset shows the temperature dependent increase of light-induced spins measured at the degradation temperatures after annealing at about 250 K (squares) compared to data of the main figure (circles). All photoinduced spin increases are shown relative to the increase at room temperature and the lines are guides to the eye.

Our degradation measurements are in substantial agreement with those obtained by Stradins and Fritzsche [47] using a technique based on photoconductivity (so-called constant photocurrent method or CPM). Previous results from photoconductivity experiments [46,47] suggested that the production of defects at 4.2 K is about 70% of the value at 300 K. We find that the production of silicon dangling bonds at 25 K is at most 50 % when compared to degradation at room temperature. In fact, within experimental error this reduction could be more than a factor of ten.

The defects that are created at low temperatures almost completely anneal at room temperature. This behavior might indicate that different defects are created at low temperatures than at higher temperatures. However, they must have the same ESR fingerprint. On the other hand, it is possible that the same defects, namely the Si dangling bonds, are created at both high and low temperatures, but that the stabilizing process is temperature dependent.

In summary, low temperature experiments that measure the production of silicon dangling bonds must take great care to remove the long-lived carriers trapped in localized band-tail states. These carriers are very difficult to remove optically. Although the temperature dependence is not strong, the production of silicon dangling bonds in a-Si:H is at most half as efficient at 25 K as at 300 K, and essentially all of the defects created after 10 h of irradiation at low temperatures (below 100 K) anneal out at 300 K. Any theoretical model must account for these facts.

Finally, we discuss the reversibility of the Staebler-Wronski effect. Figure 18 shows the spin density for the sample of a-Si:H after each successive annealing at 200°C (preliminary to each degradation measurement) and the spin density of the sample after each successive room temperature degradation process. The initial and final spin densities before and after many degradation and annealing cycles exhibit a well defined trend. Since the detected ESR signal is very sensitive to the sample position inside the ESR cavity, we again ascribe the scattering in the data mostly to slightly varying sample positions. However, slight increases of the spin densities for both the annealed sample and the degraded sample are clearly seen. The spin density of the degraded sample increases at a slower rate (in units of degradation/annealing cycles), than the spin density of the annealed sample. Therefore, the difference in the spin densities between the degraded and annealed states is decreasing. This effect, namely that the photoinduced defect creation becomes less efficient after many degradation/annealing cycles, also affects the previous data of Figs. 16 and Fig. 17. However, within the number of cycles performed in this work the error due to the production of irreversible, stable defects that cannot be annealed at 200°C is much smaller than the uncertainty in the data due to varying sample positions inside the cavity. These results indicate that the degradation of a-Si:H is not fully reversible after a large number of degradation and annealing cycles. Some photoinduced defects are stable under annealing at 200°C for 30 min, and these defects accumulate as the degradation progresses. These stable defects, i.e., those which survive annealing, cannot be distinguished by ESR from the defects that can be annealed.

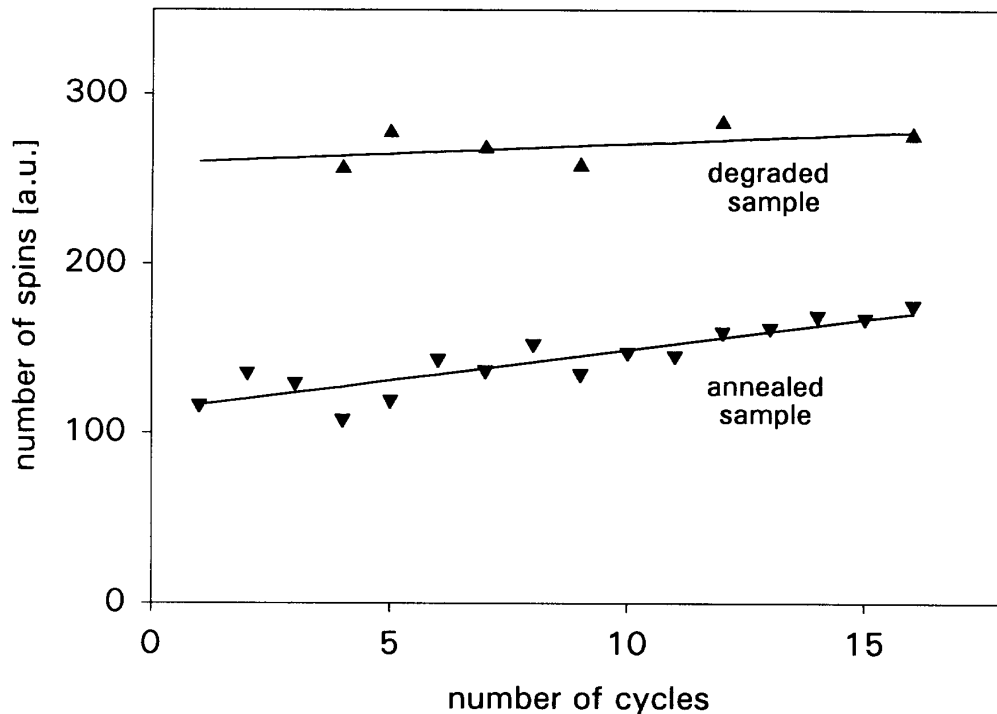

Fig. 18. Spin densities of the same sample in the annealed and degraded states are shown by the lower and upper curves, respectively. The abscissa is the number degradation and annealing cycles.

Throughout most of this section we have been discussing the production of silicon dangling bonds at low temperatures. In this discussion, the production and decay of band tail electrons and holes present competing effects that must be minimized or eliminated. However, the production of band tail electrons and holes is in itself a very interesting and important problem. In the following paragraphs we revisit this important problem.

In the field of amorphous semiconductors universal properties are rare. Perhaps the two most prominent examples are (1) the exponential dependence of the electrical conductivity on temperature, and (2) the existence of exponentially decreasing densities of localized electronic states at the edges of the electronic energy bands. Our recent experimental and theoretical studies indicate that the decay of optically excited electrons and holes in tetrahedrally-coordinated amorphous semiconductors is a universal property of these amorphous solids [27,49,53,54,55]. We have discussed this modeling in previous progress reports. Specifically, the theoretical modeling shows that at large carrier separation and long decay times (1) the random distribution of optically excited electrons and holes is subject to the condition of charge neutrality, and (2) the decays are universal and independent of the densities of localized, band-tail states. Results have been obtained on both hydrogenated amorphous silicon (a-Si:H) [27,49,53,54,55] and on hydrogenated amorphous germanium (a-Ge:H) [27,55,56,57]. At higher temperatures the results become more complicated and the decays are no longer universal but rather depend on the slopes of the conduction and valence band tails.

Shklovskii et al. [28,58] have modeled the optical excitation and subsequent decay of band-tail carriers in amorphous semiconductors at times shorter than approximately 1 ms where these processes can be monitored by the time dependence of either photoconductivity (PC) or photoluminescence (PL). As mentioned in previous progress reports, we have extended these results to the long time decays of optically excited carriers where the process must be measured by ESR since the PC and PL are much too weak. Immediately after the light is switched off the recombination is mainly geminate. The recombination rate is $\tau_r^{-1}\exp(2R/a)$, where R is the distance between the electron and the hole, a is the effective localization length, which for simplicity we assume is the same for the electron and the hole, and τ_r » 10^{-8} s. The diffusion time, t_p, which is controlled by phonons, is » 10^{-12} s, and therefore during the early stages of recombination diffusion plays the major role. At low temperatures this diffusion involves only hopping downward in energy for both the electron and the hole. When the electron and hole are separated by distances greater than $R_c = (a/2)\ln(\tau_r/\tau_p)$, the process is controlled by recombination, and diffusion can be neglected. It can be shown [49] that, regardless of the initial carrier densities, at $R > R_c$ and $t > \tau_r^2/\tau_p = \tau_r \exp(2R_c/a)$ the recombination occurs exclusively between distant pairs.

Electrons and holes are created in pairs, and therefore no pair can be separated more than R_c. For this reason, on a scale $R > R_c$ the number of electrons is equal to the number of holes, and *a model of randomly distributed electrons and holes is not relevant to describe large distances and long times*. Therefore, we have employed a simple mean field equation but imposed the condition of charge neutrality. In this case it can be shown that [49]:

$$dn(R) = -n^2(R)4\pi R^2 dR\,, \tag{5}$$

where n is the number of electrons or holes. Since the recombination at short times is geminate, we take a solution to eq. (5) of the form

$$n^{-1} - n_o^{-1} = \frac{4\pi}{3}(R^3 - R_o^3) \tag{6}$$

to eliminate these processes. In eq. (6), n_o and R_o are a density and a separation at some time where distant pair recombination clearly dominates. At large R one obtains $n(R) \cong (4\pi R^3/3)^{-1}$, which is independent of n_o. The long-time decay of the photo-excited ESR must be compared with the predictions of eq. (6). The sole adjustable parameter in eq. (6) is a, the effective localization radius. One should not take the value of this parameter too seriously because it contains the uncertainty in the absolute values of the ESR intensities. [The relative values are very well known.] In practice, one fits the decay curve for the optically induced ESR at low temperatures for a specific value of the excitation intensity. The curves for all other excitation intensities must fit the experimental data with no remaining parameters to adjust.

A representative curve for the decay of the optically induced ESR at low temperatures in a-Si:H is shown in Fig. 19. Similar growth curves are shown for a-Ge:H in Fig.9 above. This curve is shown for a specific excitation intensity (~ 20 mW/cm^2), but curves for excitation intensities between 100 mW/cm^2 and 10 nW/cm^2 fit the data very accurately with no additional adjusting of the parameter, a [49]. The value of a used in Fig. 19 is 2.4 x 10^{-7} cm, but this value is not accurate since it contains the inherent uncertainty in the absolute value of the ESR spin density, which is at best a factor of three.

Similar agreement is obtained for optically excited ESR in a-Ge:H [56,57]. In this case, the spin-lattice relaxation times are short enough that the standard ESR detection scheme can be employed, and one observes the derivative of the ESR absorption (See Fig. 7 above).

Although the curves are universal, and in particular independent of the slopes of the conduction and valence band tails, as the temperature approaches zero, at finite temperature the band-tail slopes begin to influence the decay processes. Practically speaking, this temperature is approximately 80 to 100 K in a-Si:H.

Although the modeling outlined above provides an excellent description of the time decay of the optically excited band-tail carriers at low temperatures, this description provides no microscopic understanding of the wavefunctions of these states (other than perhaps an order-of-magnitude estimate of the localization radius, a). For this reason, we turn to paramagnetic states

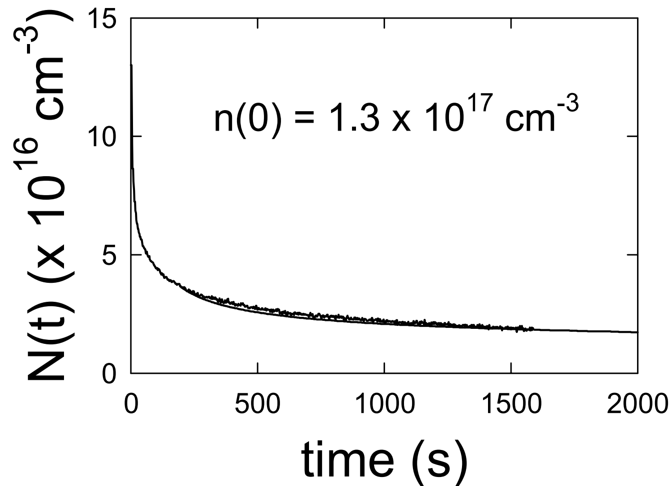

Figure 19. Decay of the optically induced ESR detected using the second harmonic technique. Data are taken at 40 K after saturation at an excitation intensity of 19 mW/cm^2. The solid line is a theoretical fit to the data using eq. (2). See text for details.

in crystalline Si (c-Si) where, for many reasons, the details are much better understood. One important defect in c-Si is the divacancy. This defect, which consists of two adjacent, missing Si atoms, is diamagnetic in its neutral state. However, when the divacancy is either positively or negatively charged, the defect becomes paramagnetic. In c-Si, one can charge the divacancies by simply moving the Fermi level by doping or, in principle, by charge injection. Because these defects are well oriented in a periodic lattice, their properties can be studied in detail by mapping

the ESR spectrum as a function of the orientation of the divacancy with respect to the applied magnetic field. Additional information is obtained from the so-called hyperfine interaction of the paramagnetic spin with ^{29}Si atoms that appear randomly on the surface of the divacancy. The relative abundance of ^{29}Si is approximately 5%.

The ESR parameters that characterize the electron (negative charge state) and hole (positive charge state) localized on the divacancy in c-Si:H are given in Table 2 [59]. The g-tensors are anisotropic but nearly axially symmetric along the long axis of symmetry of the divacancy (parallel to the line of centers between the two missing Si atoms). The hyperfine interaction with ^{29}Si is predominantly with two equivalent Si atoms near the divacancy.

Even if there exists the analog of a divacancy in a-Si:H, these defects would be expected to be arranged randomly within the amorphous film. As a first order comparison, we therefore take a powder average (average of the ESR spin-Hamiltonian over all equally-probable angles of the g- and hyperfine tensors with respect to the applied magnetic field) of the spectrum for c-Si as an approximation to that which may occur in the amorphous form. We assume equal numbers of negatively and positively charged divacancies corresponding to equal numbers of trapped electrons and holes. Figure 20 shows the agreement between this approximation and the

Table 2. ESR Parameters for the Charged Divacancy in Crystalline Si

Positively Charged	Negatively Charged
$g_1 = 2.0004$	$g_1 = 2.0012$
$g_2 = 2.0020$	$g_2 = 2.0135$
$g_3 = 2.0041$	$g_3 = 2.0150$
$A_{\parallel} = 67.8\ cm^{-1}$	$A_{\parallel} = 79\ cm^{-1}$
$A_{\perp} = 40.0\ cm^{-1}$	$A_{\perp} = 56\ cm^{-1}$

experimentally observed optically induced ESR in a-Si:H. The dashed line ignores the hyperfine interaction with ^{29}Si, and the solid line contains this interaction. Figure 21 contains the same three curves on an expanded scale to emphasize the regions where the ^{29}Si hyperfine might be expected to occur. In Fig. 22 we make the same comparisons with the standard derivative ESR lineshape for optically excited, band-tail electrons and holes.

At low temperatures in a-Si:H, two optically induced ESR signals occur, whose characteristic g-values are approximately 2.004 and 2.01. These signals are usually attributed to electrons trapped in localized conduction-band-tail states and holes trapped in localized valence-band-tail states, respectively [60]. In addition to these two optically induced ESR signals, there is a third, metastable ESR signal centered at g = 2.0055 that is attributed to neutral silicon dangling bonds. Because of the small difference in g-values, it is often difficult to separate this latter signal from that attributed to band-tail electrons. Although this detail may affect the lineshape analysis, it is of no consequence to the decays, such as that shown in Fig. 19, because one can monitor the time dependence of the signal in a region that is unambiguously due to either the band-tail electrons or the band-tail holes.

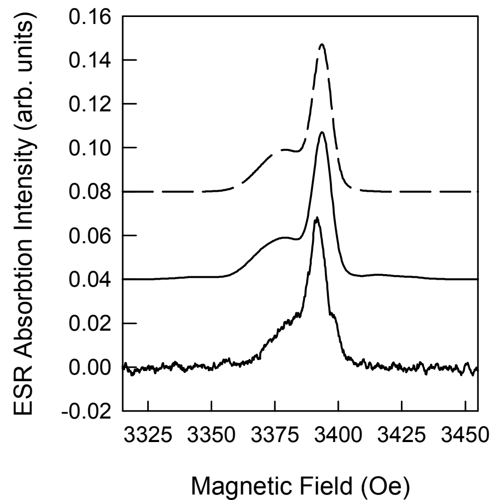

Figure 20. (Left Side) Comparison of experimental optically induced ESR spectrum at 40 K (bottom curve) as detected using the second harmonic technique with calculated powder spectra for the negatively and positively charged divacancy in crystalline silicon. The dashed line and solid line are spectra without and with the ^{29}Si hyperfine of the divacancy, respectively. See text for details.

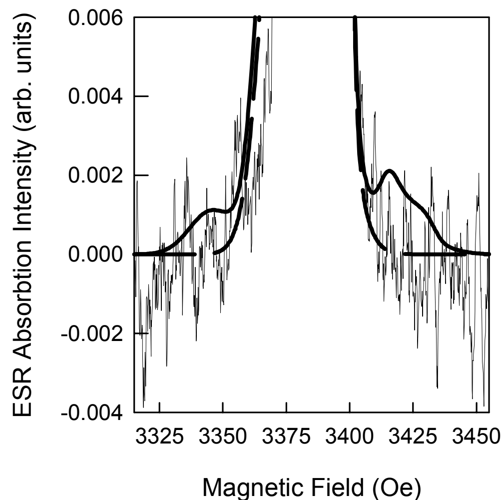

Figure 21. (Right Side) Comparison of experimental optically induced ESR spectrum at 40 K (noisy curve) as detected using the second harmonic technique with calculated powder spectra for the negatively and positively charged divacancy in crystalline silicon on an expanded scale. The dashed line and solid line are spectra without and with the ^{29}Si hyperfine of the divacancy, respectively.

Umeda et al. [61] have used pulsed optically induced ESR measurements in samples of a-Si:H with different concentrations of ^{29}Si to infer that the wave function of the trapped electrons is consistent with an antibonding orbital highly localized at a single Si-Si bond. These authors also speculated that the hole was similarly localized at a single Si-Si bond. The comparisons shown in Figs. 20 through 22 clearly indicate that the ESR lineshapes are also consistent with localization over a larger volume. In addition, recent calculations of Fedders et al. [62] suggest that the band-tail electrons and holes are delocalized over at least several atoms. These calculations also exhibit the quasi-one-dimensional aspect exhibited by the wavefunctions for the

charged divacancy in crystalline Si. Indeed, these are the only two features that the comparisons shown in this paper support. One should not infer from Figs. 20 through 22 that divacancies exist in a-Si:H but rather that the localization and asymmetry of the wavefunctions for band-tail states in a-Si:H are similar to those that occur at charged divacancies in crystalline Si.

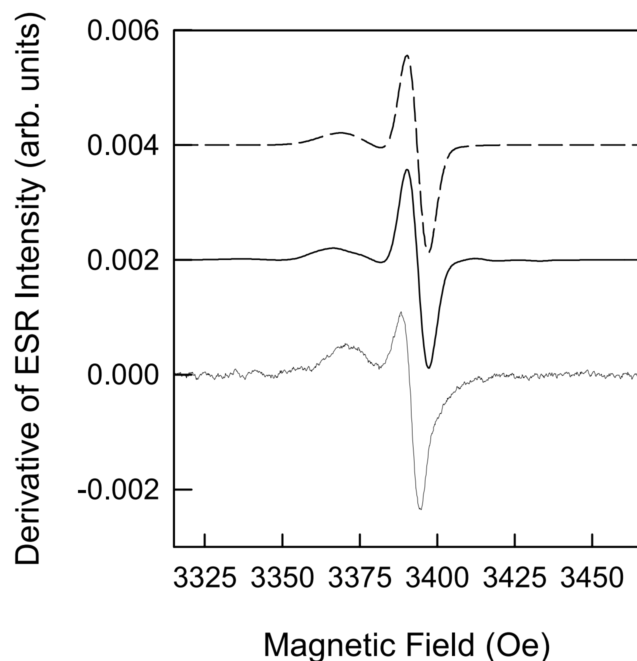

Figure 22. Comparison of experimental optically induced ESR spectrum at 40 K (bottom curve) as detected using the standard detection technique (which produces a derivative of the ESR signal) with calculated powder spectra for the negatively and positively charged divacancy in crystalline silicon. The dashed line and solid line are spectra without and with the ^{29}Si hyperfine of the divacancy, respectively.

With regard to the hyperfine interaction with ^{29}Si nuclei, one can say very little because of the poor signal to noise ratios of the experimental traces in the spectral regions where this effect should manifest itself. This interaction must clearly exist, but variations from site to site will probably wash out any resolved structure.

ESR experiments at low temperatures ($T < 50$ K) in a-Si:H and a-Ge:H show that the decay of optically excited electrons and holes in tetrahedrally-coordinated amorphous semiconductors is a universal property of these amorphous solids. Specifically, these decays are independent of the slopes of the conduction and valence band tails. Comparisons of the ESR lineshapes attributed to band tail carriers in a-Si:H with those calculated for randomly oriented, charged divacancies in crystalline Si suggest that the wavefunctions in a-Si:H are localized over more than a single strained bond and that they are probably elongated in one direction.

6. DIRECT DETECTION OF MOLECULAR HYDROGEN BY ^{1}H NUCLEAR MAGNETIC RESONANCE

The presence of molecular hydrogen in a-Si:H has been an important issue since the early studies. However, both the concentration and the local environment of H_2 are controversial due to the difficulty of detecting ortho-molecular hydrogen (o-H_2) directly. During this quarter we have employed a new way to measure the concentration and to investigate the local environments of o-H_2 in a-Si:H by ^{1}H NMR.

It is well known that the NMR lineshapes of bonded hydrogen in a-Si:H consist of a narrow line (~ 4kHz) due to dilute hydrogen and a broad (~ 20 kHz) line due to clustered hydrogen [63,64,65]. In addition, small portion of hydrogen exists in form of molecular hydrogen in a-Si:H [63,66]. ^{1}H NMR is sensitive only to ortho-hydrogen (o-H_2) since para-hydrogen (p-H_2) has total nuclear spin I = 0. Ortho-hydrogen (o-H_2) has total nuclear spin I =1 and rotational angular momentum J = 1. The three rotational states ($m_J = 0, \pm 1$) are degenerate for isolated o-H_2. The degeneracy can be lifted in solids due to the anisotropic crystal field, with non-degenerate $m_J = 0$ state as the lower energy state and two-fold degenerate $m_J = \pm 1$ states as upper states. The energy splitting D depends on the EQQ interaction between o-H_2 and the interaction between EFG from the lattice and electric quadruple moment of o-H_2. When $kT \ll kT_c = D$, the o-H_2 molecules are frozen in the lower $m_J = 0$ state, i.e., they are locally ordered with respect to their local field, the resultant NMR lineshape is a powder averaged Pake doublet with splitting dn = 173 kHz [66,67,68]. This provides a unique fingerprint of o-H_2 molecule. However, at higher temperature ($kT \gg kT_c$) the o-H_2 molecules are tumbling very fast and the Pake doublet is motionally narrowed to an unresolved central line. For solid hydrogen, $T_c \sim 1.6$ K, but T_c can be as high as 20 K in a-Si:H [66]. This is mainly due to the additional EFG from the Si lattice. As one can see, the EFG contributes to most of the energy splitting in a-Si:H.

In principle, one can observe the Pake doublet from free induction decay (FID) following a 90^0 pulse. However, in practice, this method suffers severely from the receiver recovery time due to the broad spectrum of o-H_2. Also, the low concentration of o-H_2 makes it difficult to distinguish it from bonded hydrogen. For this purpose, the Jeener-Broekaert three-pulse where T_2 is the spin-spin relaxation time and T_{1d} is the dipolar spin-lattice relaxation time. Since bonded hydrogen and o-H_2 have different T_2 and T_{1d}, one can selectively emphasize a certain component and measure the concentration more accurately.

One PECVD sample and three HWCVD samples are measured at T=8 K. Figure 23 shows the typical spectra in frequency domain. It can be seen that the Pake doublet for PECVD sample is well defined and no motional narrowing is observed. However, the HWCVD sample shows strong motional narrowing as evident from the narrowed central line of ~ 70 kHz and much less prominent Pake doublet. Since the local field is mainly determined by the EFG from Si lattice, this indicates a more ordered Si lattice in the HWCVD samples, which has been suggested by internal friction measurements [69]. Sequence (JB sequence hereafter) was used.

A JB sequence consists of a 90^0 pulse followed by a pair of 45^0 pulses that are 90^0 phase shifted [70]. The time interval between the first, second and third pulse is τ_1 and τ_2, respectively. At $t=\tau_1$ after the third pulse, a stimulated echo forms, the amplitude of the stimulated echo can be expressed as [71]:

$$f(\tau_1, \tau_2) \propto e^{-2\tau_1/T_2} e^{-\tau_2/T_{1d}} \quad , \tag{7}$$

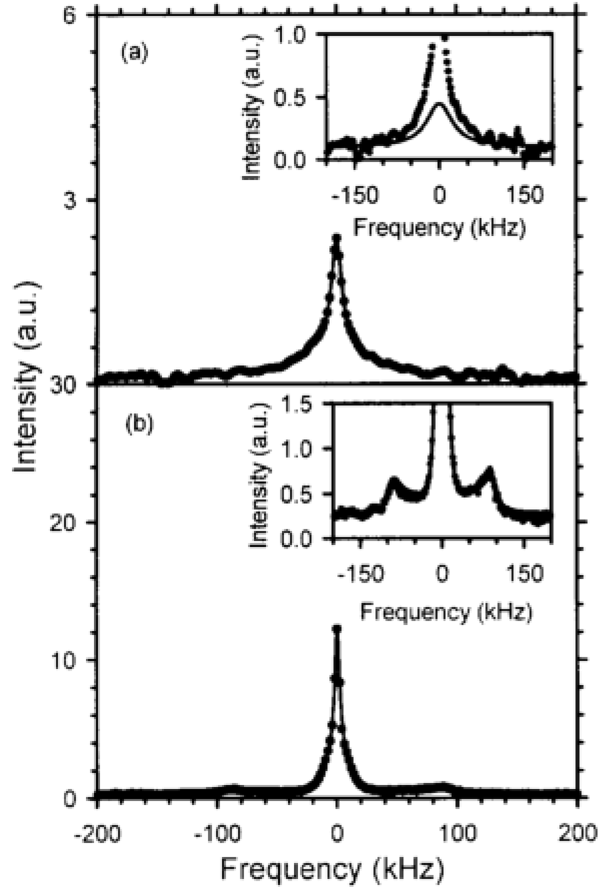

Fig. 23. FT spectrum of the stimulated echo for a PECVD sample and an HWCVD sample at T = 8 K. (a) HWCVD sample: The solid circles are the data. The solid line is the fit. The Pake doublet has narrowed to a ~70 kHz central line. The inset shows the 70 kHz line and the corresponding fitting on an expanded scale. (b) PECVD sample: The solid circles are the data. The solid line is the fit. The inset shows the Pake doublet on an expanded scale. The splitting of the Pake doublet is 176±5 kHz.

Figure 24 shows the dependence of t_1 of the three components with $\tau_2=0$, the total intensity has been normalized to one at $\tau_1=\tau_2=0$ to show directly the signal fractions. It is found that o-H_2 molecules contribute about 10% of the total hydrogen signal. On the other hand, the minimum of spin-lattice relaxation time (T_1) of bonded hydrogen is measured, and the o-H_2 fraction was inferred to be only about 1 % of total hydrogen. Similar results were obtained for HWCVD samples. In these samples, the JB sequence yields ~1% of total hydrogen as o-H_2, while that inferred from the T_1 minimum of bonded hydrogen is at most 0.1%. In fact, the T_1 of bonded hydrogen is almost independent of temperature, indicating perhaps a different spin-lattice relaxation mechanism.

Clearly, most of the o-H_2 molecules do not participate in the spin lattice relaxation of bonded hydrogen. To further understand the discrepancy, T_1 of o-H_2 was measured at T=40 K where the T_1 minimum of the bonded hydrogen occurs. Figure 25 shows the results. One can see clearly that two very different T_1 values are present. The longer one (~ 0.6 s) is essentially independent of temperature and may be due to the EQQ interaction between hydrogen molecules as in solid hydrogen, therefore these o-H_2 do not relax the bonded hydrogen. The shorter T_1 (~ 3 ms) is very close to the value calculated assuming a two phonon Raman process, which is believed to induce the relaxation of bonded hydrogen. It can be seen that only a small portion (~ 30 %) of the o-H_2 molecules can relax the bonded hydrogen, hence the different o-H_2 fraction from two different methods mentioned above. This experiment has provided the first direct evidence for two different o-H_2 environments. However, one should notice that the EQQ induced T_1 (~ 0.6 s) doesn't necessarily indicate the presence of large voids as proposed earlier [72]. Since the distance between o-H_2 in two adjacent interstitial T-sites (~5 Å) is close to that in solid hydrogen, it is possible that o-H_2 molecules trapped in adjacent T-sites relax via the EQQ interaction.

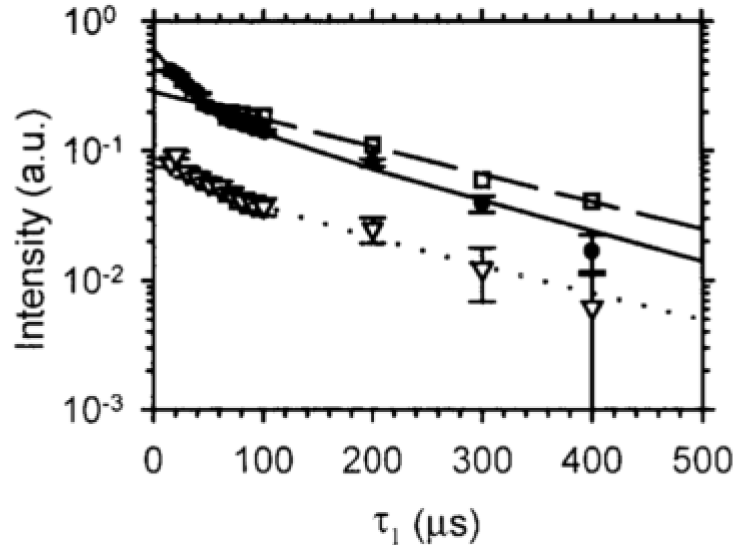

Fig. 24. The τ_1 dependence of the signal intensities for $\tau_2 = 0$. Open squares, solid circles and open triangles represent the Lorentzian, Gaussian and o-H_2 components, respectively. The dashed line, solid line and dotted line represent the corresponding fits. The short values of T_2 for the Gaussian and o-H_2 components are 59 and 66 μs, respectively. The long values of T_2 are about 400 μs for all components.

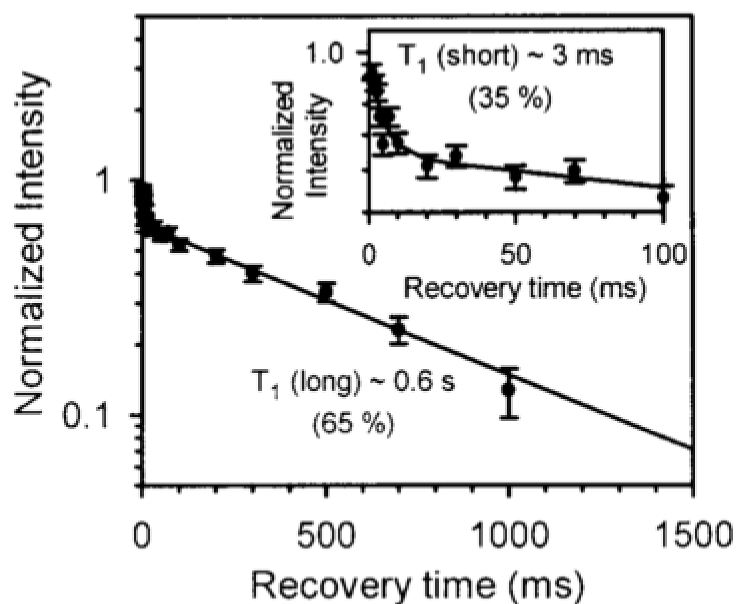

Fig. 25. The o-H_2 signal intensity as a function of recovery time after a saturating comb of pulses. The signal is normalized to I (t = ∞). The shorter T_1 is about 3 ms. The longer T_1 is about 0.6 s. The signal fractions of the two components are 35 % and 65 % respectively.

The Deuterium NMR(DMR) of a-Si:H,D and a-Si:D has raised the question whether the whole 4 kHz narrow line (~30% of total hydrogen) is due to the molecular hydrogen in the interstitial sites [73]. To investigate the relation between the narrow line and o-H_2, the signal fraction of bonded hydrogen was measured by fitting the FID. Figure 26 compares the lineshape in the time domain at room temperature and at T=8 K for PECVD samples. The ratio between the broad Gaussian and the narrow Lorentzian is found to be 60 % vs. 40% at room temperature and 60 % vs. 30 % at 8 K, with 10 % of the signal from o-H_2 molecules. The slightly different line width of the narrow line is within the experimental error. These data suggest that the signal from o-H_2 (10 %) is narrowed into the narrow line at room temperature, perhaps with a slightly different line width, but only contributes to ~ 25 % of the narrow line. This number is consistent with the earlier report by Boyce and Stutzmann [66].

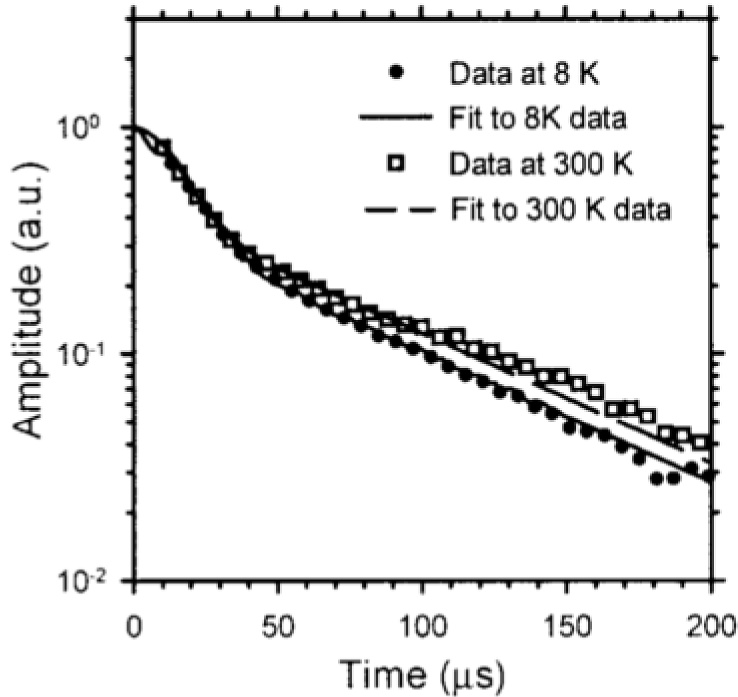

Fig. 26. Comparison of FID at T = 300 K and T = 8 K. The sold line is the observed FID at 8 K on which is superimposed 10 % of the o-H_2 signal. The signal fractions of the 20 kHz and 4 kHz central lines are 60 % and. 30 % at 8K and 60% and 40 % at 300 K.

Although the results from DMR strongly suggest that the whole 4 kHz narrow line (~30% of total hydrogen) is due to molecular hydrogen, there is evidence that is difficult to be explained by such a suggestion. First, the narrow line persists even at T=1.4 K, and its fraction (~ 40 %) is almost independent of temperature below T_c ~ 20 K. This result suggests that most o-H_2 molecules, if they contribute to the narrow line, have to reside in those sites with negligible EFG from the Si lattice so that they "never" freeze. But this scenario is unlikely for an amorphous material since the EFG is highly sensitive to the structure of the lattice. Second, hole-burning experiments show that the intrinsic line width of the narrow line is ~ 0.5 kHz [74]. Therefore, there must be significant clustering of o-H_2 to broaden the line to 4 kHz (due to the much smaller gyromagnetic ratio of o-H_2). With this amount of clustering the resultant local density of o-H_2 molecules could be as high as 20 to30 at. %. Since the Si lattice constant (~2.5 Å) is much smaller than that of solid hydrogen (~ 3.9 Å), the resultant EQQ interaction between o-H_2 in a-Si:H can be comparable to that in solid hydrogen. This value for EQQ sets a lower bound for T_c that is close to that in solid hydrogen (T_c ~1.6 K). The third and most important evidence is from ortho-para conversion experiments [63], where the isolated o-H_2 concentration is reduced by more than a factor of five by storage at liquid helium temperatures for many months. The clustered o-H_2 converts much faster than isolated o-H_2. If the local density of o-H_2 were as high as 20 to 30 at. %, one would expect the total concentration of o-H_2 to be reduced much more than factor of five. In addition, the intensity of the narrow line would be reduced to less than 5% of total signal, a reduction that is not observed in the experiments.

The experimental results and arguments discussed above suggest that part of the narrow line is due to o-H_2 molecules, but that most of the narrow line comes from the dilute hydrogen that is bonded to silicon.

In conclusion, the concentration of molecular hydrogen in a-Si:H is much higher than previously believed. Most o-H_2 molecules do not participate in the spin-lattice relaxation of bonded hydrogen. Two o-H_2 environments exist, one in which the molecules are essentially isolated and one in which the molecules are clustered. Part of the 4 kHz narrow line at room temperature is due to o-H_2 molecules. Finally, the o-H_2 lineshape in HWCVD samples suggests a more ordered structure for the Si lattice than in typical PECVD samples.

Because the HWCVD films are very different than the standard PECVD films in many respects, it is important to determine the microscopic mechanisms that produce these changes in the electronic, optical, and micro-structural properties. Figure 27 shows the difference in the

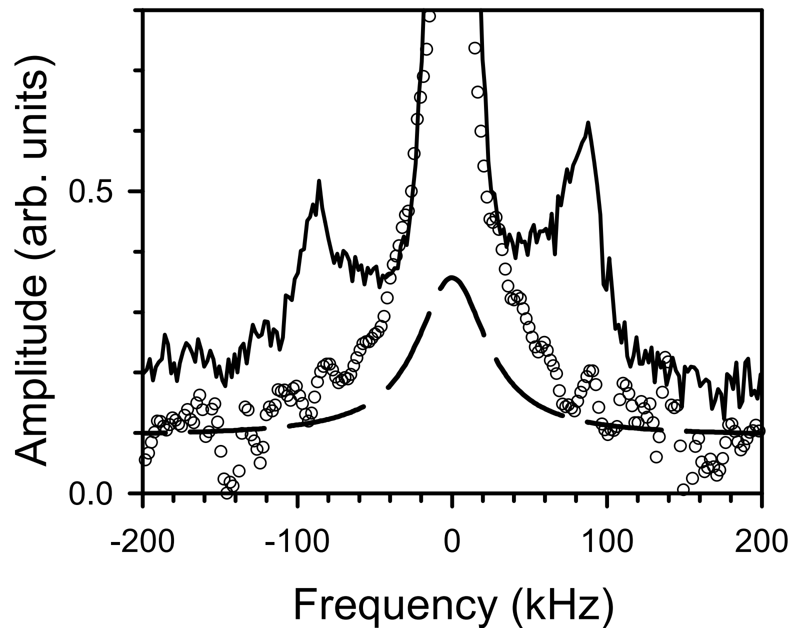

Figure 27. Comparison of the ortho-molecular hydrogen lineshape for the PECVD and HWCVD samples at T = 8 K. The solid line and open circles represent the data for the PECVD and HWCVD samples, respectively. The dashed line is a fit to the narrowed Pake doublet for a HWCVD sample. The width of the fitted line is ~70 kHz FWHM.

molecular hydrogen NMR (Jeener-Broekaert stimulated echo) signal at low temperature where the molecular hydrogen in the PECVD sample is well defined because the molecules are "frozen". In the HWCVD sample the molecular hydrogen signal is less well defined because the molecules are still rotating. Above, we interpreted this behavior as evidence for a more ordered Si network in the HWCVD films [75].

In contrast to the typical PECVD samples, which exhibit a strong temperature dependent $T_1(H)$, the HWCVD samples have $T_1(H)$ that is weakly dependent on the temperature and much longer at the temperature where the minimum in $T_1(H)$ is expected. For the HWCVD samples, $T_1(H)$ is approximately equal to 5 s at T = 40 K, where the minimum is expected. This value is about one order of magnitude larger than that of the typical PECVD samples. One possible mechanism for such a behavior is the relaxation through rapidly relaxing paramagnetic centers, such as silicon dangling bonds. However, an estimated density of dangling bonds of $\sim 10^{18}$ cm^{-3} is needed to produce such a value. This density is much too large for these materials. Another possibility is that the bonded hydrogen relaxes through those clustered molecular hydrogen molecules, which relax through a temperature independent electric quadruple-quadruple (EQQ) interaction. Nevertheless, for EQQ induced relaxation [$T_1(H_2) \simeq 0.6$ s], the concentration of ortho-molecular hydrogen must be ~ 10 % of the total hydrogen to produce a $T_1(H)$ of ~5 s. As mentioned above, this concentration is about one order of magnitude higher than is observed. The third possibility is spin-diffusion limited relaxation through those ortho-molecular hydrogen molecules that have a phonon-induced T_1 of ~3 ms. In this case, T_1 for spin diffusion, $T_{1(SD)}$, is [76]

$$T_{1(SD)}^{-1} = 4\pi D \frac{3}{4} n(H_2) b, \tag{8}$$

where b is the average distance between an ortho-molecular hydrogen molecule and the nearest bonded H, and $n(H_2)$ is the concentration of ortho-molecular hydrogen that contributes to $T_1(H)$. D is the spin-diffusion constant, and one calculation gives D as [77]

$$D = d^2 \frac{d^2}{30 < T_2 >}, \tag{9}$$

where d is the average distance between bonded hydrogen atoms and $<T_2>$ is the averaged T_2 for the entire NMR line. However, this formula, which applies to a homogeneous system, is not particularly appropriate for the HWCVD samples. In these samples, a large portion of the hydrogen is heavily clustered with a $<T_2>$ much smaller than that of the PECVD sample, even though the hydrogen concentration is much lower than that of PECVD samples. A more refined model [78], due to Fedders, is also inappropriate because of the inhomogeneous distribution of hydrogen atoms.

As a consequence, we argue that the diffusion time in HWCVD samples is mainly determined by the diffusion among the dilute hydrogen atoms, and therefore the average T_2 should be taken as the average of the narrow line that arises from the dilute hydrogen. Although the nuclear spins can quickly thermalize within the cluster, as reflected by the much shorter T_2 of the broad line, it will take much longer time for the spin to diffuse beyond the cluster. This argument is similar to that concerning the region near an ortho-molecular hydrogen in the case of diffusion limited relaxation [78], where the details of the diffusion near an ortho-molecular hydrogen are not important as long as the concentration of ortho-molecular hydrogen is small. A more general discussion of spin-diffusion can be found in [79].

For the HWCVD samples supplied by NREL, the hydrogen concentration is ~3 at. %, and about 70 % of the hydrogen is in clustered sites. If we treat each of these clusters as a single site that quickly thermalizes, then the effective concentration is ~2 at. %, which yields b ≈ d ≈ 6 Å. A hole-burning experiment gives an intrinsic line-width, δ of ~0.5 kHz for the narrow line [80], which sets the scale of the dipolar interaction, and therefore the transfer rate of magnetization between two adjacent spins. A rough estimate of the $\langle T_2 \rangle$ of the dilute hydrogen is

$$\langle T_2 \rangle = (\pi\delta)^{-1} \approx 700\ \mu s \tag{10}$$

By taking $n(H_2)$ to be at most 0.1 % of the total hydrogen, $T_{1(SD)}$ is estimated to be at least 5 s. On the other hand, for the same $n(H_2)$, at T = 40 K, the relaxation time through ortho-molecular hydrogen, is ~1.5 s. This value is smaller than $T_{1(SD)}$ estimated above. Such a qualitative estimate suggests that the relaxation process in the NREL HWCVD samples is probably spin-diffusion limited, resulting in a weak temperature dependence.

In summary, the comparison of the lineshapes at 8 K between the PECVD and HWCVD samples suggests that the HWCVD samples have a more ordered silicon matrix. The spin-lattice relaxation mechanism for bonded hydrogen in the HWCVD samples is probably limited by spin diffusion in the bonded hydrogen system.

Under a previous sub-contract we showed [81,82] that the dipolar spin-lattice relaxation of bonded hydrogen, depends on the defect concentration and doping of the materials. Since the signal to noise ratio limited the measurement to the short time region of T_{1d}, these results showed exponential behavior. The dipolar spin-lattice relaxation was ascribed to the local motion of these hydrogen atoms. However, there are some difficulties in relating the relaxation to local motion of the hydrogen. First, it is found that for temperatures below 200 K, both the long T_{1d} and the short T_{1d} are almost independent of the temperature [83]. At 8 K, the value of the short T_{1d} is almost the same as that at 300 K, while a thermally activated process would result in a much longer T_{1d}. Second, there is no motional narrowing of the bonded hydrogen up to room temperature. Therefore, the time between two jumps of a spin, τ_c cannot be estimated by $\tau_c \approx T_2$ [81,82]. Moreover, T_{1d} strongly depends on the (silicon neutral dangling bond) defect density or doping level. Since the defect density (~10^{15} cm^{-3}) is much lower than the hydrogen concentration(~10^{21} cm^{-3}), it is difficult to understand how such a small concentration of electrons can influence the motion of so many hydrogen atoms.

On the other hand, as shown in Fig. 28, the dipolar spin-lattice relaxation during τ_2 is not exponential. Similar behavior is also found in [83]. Although a phenomenological fit with two values of T_{1d} gives satisfactory agreement with the experimental data, the underlying physical mechanism is not clear. In particular, it is not clear why both the narrow line and the broad line exhibit similar values of T_{1d}, despite their very different environments. We found that such a non-exponential decay can be fitted by assuming that the intensity of the decay is given by

$$I(\tau_2) \cong \exp\left\{-(\tau_2/\tau)^{1/2}\right\} \tag{11}$$

as shown in Fig. 29. The values of τ are 7.3 ms and 8.6 ms for the Lorentzian and Gaussian components, respectively. These values are identical within experimental error. This behavior is well known for the case of spin-lattice relaxation by paramagnetic centers without spin diffusion [84,85], and the non-exponential behavior is due to inhomogeneous relaxation [86]. In the following paragraphs we outline an alternative interpretation to local motion, one that incorporates the dependence of T_{1d} on the defects and doping in a more natural manner. Although admittedly crude, this approach sheds some light on the further understanding of the phenomenon.

A typical PECVD sample contains density of paramagnetic defects of $\sim 10^{15}$ cm^{-3}. These defects can be detected by electron-spin-resonance (ESR). The average distance between two electrons is $d_e \simeq 10^{-5}$ cm. The total Hamiltonian including both the nuclei and electrons is

$$H = H_{ZI} + H_{ZS} + H_{DII} + H_{DIS} + H_{DSS} \quad (12)$$

where $\mathbf{H_{ZI}}$ and $\mathbf{H_{ZS}}$ are the Zeeman Hamiltonians for the nuclei and electrons, respectively. The last three terms represent the secular part of the total dipolar Hamiltonian of the system. $\mathbf{H_{DII}}$ and $\mathbf{H_{DSS}}$ are nuclear-nuclear and electron-electron dipolar energies, respectively, and $\mathbf{H_{DIS}}$ is the dipolar interaction between the nuclei and the electrons. For systems with two types of spins, the total dipolar energy, including interactions between both like and unlike spins, is a constant of the motion [87]. Therefore, the electrons and the hydrogen atoms form a single dipolar reservoir that, at internal equilibrium, has a common dipolar spin temperature. (A detailed discussion of the thermodynamics of the spin system is given by Jeener et al. [88].) Right after the second pulse of the Jeener-Broekaert (JB) sequence, the dipolar energy of the hydrogen atoms increases, but the entire dipolar system, including both electrons and the hydrogen, is far from internal equilibrium. During the time following the second pulse, the dipolar energy is redistributed between the hydrogen atoms and the electrons to establish a common dipolar spin temperature. Because the electronic dipolar system is initially at the lattice temperature, such a process effectively cools the nuclear dipolar system. During this cooling the dipolar energy of the nuclear system decreases and the dipolar energy of the electronic system increases. Such behavior has been reported for LiF where after preparing the dipolar order in the ^{19}F system, a simultaneous decrease of ^{19}F dipolar energy and increase of ^{7}Li dipolar energy is observed [89]. If the spin diffusion between nuclei is rapid compared to the rate of energy exchange between the nuclei and the electrons, the time needed to reach an internal equilibrium is determined by the relative heat capacities of the nuclear and the electronic dipolar systems. In this case, a characteristic time τ_c is of the form similar to that derived for spin lattice relaxation due to molecular hydrogen [75]. However, using d_e estimated above, a spin-diffusion bottleneck is estimated to occur at $\sim 10^5$ s, much larger than the experimentally observed value. Therefore the relaxation will be determined by the direct rate of energy exchange between each nuclei and the electrons, a process in which spin diffusion is not important.

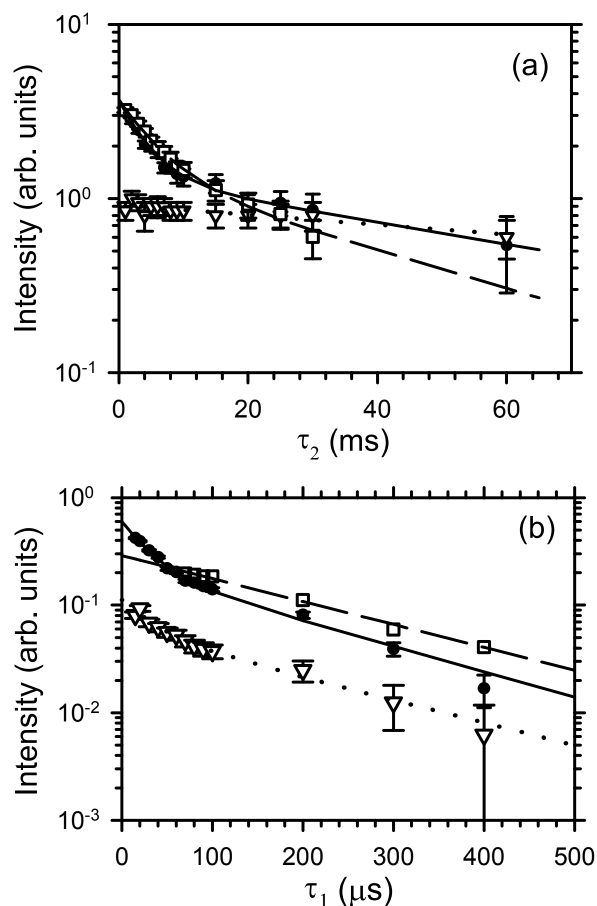

Figure 28. The dependence of the intensities on τ_1 and τ_2 for the broad, narrow, and ortho-molecular hydrogen components of the PECVD sample. Solid circles, open squares, and open triangles represent the broad, narrow, and ortho-molecular hydrogen components, respectively. The solid line, dashed line, and dotted line are the corresponding fits to the broad, narrow, and ortho-molecular hydrogen components, respectively. (a) Dependence of intensities on τ_2. For the broad and narrow lines. The values of the shorter T_{1d} are ~4 and 6 ms, respectively. The values for the longer T_{1d} are ~70 and 40 ms, respectively. The T_{1d} for ortho-molecular hydrogen is ~150 ms. (b) Dependence of the intensities on τ_1 for $\tau_2 = 0$. The value of the longer T_2 is ~400 μs for all three components. The values of the shorter T_2's are ~60 and 70 μs for the broad line and the Pake doublet, respectively.

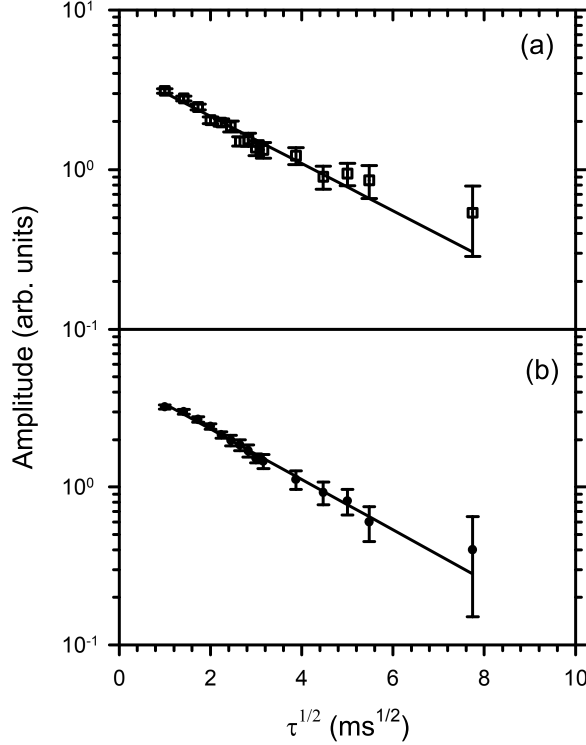

Figure 29. Fit to the τ_2 dependence of the echo intensity according to Eq. (1). (a) Fit to the Gaussian component, and (b) fit to the Lorentzian component. Open squares and solid circles represent Gaussian and Lorentzian components, respectively. Solid lines are the corresponding fits. The values of τ are 8.6 ms and 7.3 ms for the Gaussian and Lorentzian components, respectively.

The above process can occur under two scenarios. If the electrons have good thermal contact with the lattice, then the approach to internal equilibrium in the dipolar reservoir will be controlled effectively by the dipolar spin-lattice relaxation of the entire system. If not, then one would expect first the establishment of the internal equilibrium discussed above, and then the entire dipolar reservoir will relax toward the lattice temperature, with a time scale much longer. In either case, the initial decrease of the dipolar signal of the nuclei will depend on the concentration of the paramagnetic electrons, which is related to silicon dangling bond density and the doping level. For a-Si:H, the first situation is most likely because the spin-lattice relaxation time of the electrons is much shorter than that of the hydrogen ($T_1 \simeq 10$ ms at 8K) [90,91]. Any calculation of the dependence on the electron density is complicated by the fact that the dipolar interaction between nuclei and electrons varies over a wide range. However, Stöckmann and Heitjans [86] pointed out that, for the case where spin-diffusion is not important, Eq. (11) generally holds if the coupling constant a(r) takes the form

$$a(r) = a_0 \left[\frac{r_0}{r} \right]^6 \quad (13)$$

where r_0 is the distance between the defect and its nearest neighbor and a_0 the corresponding coupling constant. The distance, r, is between the defect and the reference nucleus. In this case τ, defined in Eq. (11), will be proportional to N_p^{-2}, where N_p is the density of paramagnetic defects. Using the data reported in [81,82], the ratio of defect density before and after light-soaking is $N_p^{(i)} / N_p^{(f)} \approx 1/2$. The corresponding ratio of T_{1d} is $T_{1d}^{(i)} / T_{1d}^{(f)} \approx 3$, which qualitatively agrees with the argument presented above. Several experiments can be performed to test this interpretation. One is to illuminate the sample at low temperature to create large amount of the paramagnetic electrons and holes trapped in band-tail states. If the above argument is correct, this dramatic increase in N_p should result in a significant reduction of T_{1d} as expected. Also one may disturb the electronic system by applying a microwave field at the resonance frequency of the electrons after the second pulse, and monitor the effect on the nuclear dipolar order. The third experiment is to measure $T_{1\rho}$, the spin-lattice relaxation time in the rotating frame, which should depend on the NMR frequency, ω, as ω^{-2} and on the time as shown in Eq. (11). On the other hand, motion-induced relaxation should be independent of the field. The fourth experiment is an electron-nuclear double-resonance (ENDOR) experiment. If one can measure the dipolar signal of the electrons, then by preparing the nuclear system with dipolar order and monitoring the electronic signal, the change of the electronic dipolar energy should be observable.

In summary, the non-exponential dipolar relaxation probably reflects an approach to the internal equilibrium of the entire dipolar system including both nuclei and electrons. Therefore, this relaxation depends quite naturally on the defect density and the doping level.

7. GROWTH OF FILMS AND P-I-N SOLAR CELLS

The three-chamber PECVD system, which was up-graded just prior to the initiation of Phase I of this sub-contract, has been routinely making films of intrinsic and doped a-Si:H from very early on in the first phase. Using hydrogen dilution, we have made films that span the range from amorphous to microcrystalline micro-structures. Films of intrinsic and doped a-Si:H have been supplied to several groups for various investigations, including (1) samples to Professor Tolk at Vanderbilt University for low energy PLE experiments using the Free Electron Laser facility, (2) samples to Professor Hari at California State University, Fullerton, for high field, ultra-low-temperature NMR studies at the National High Magnetic Field Laboratory (Gainesville, FL), (3) samples of microcrystalline and nano-crystalline a-Si:H to Professor Inglefield at Weber State University for atomic force microscopy of the micro-structure, and (4) samples to Professor Vaseashta at Marshall University for transport measurements of stability.

In Phase II we initiated growth of p-i-n cells, which employ the a-Si:H materials system. Cells with moderate efficiencies (7 to 8 %) have been made in Phase III, and improvements are being pursued to increase the efficiencies. In Phase III we have also made efficient cells using amorphous silicon-sulfur alloys in the i-layers. We have purposely made both the control cells, where the i-layers contain no sulfur, and the sulfur containing cells with thick i-layers (~1 μm) to enhance the degradation due to the Staebler-Wronski effect. For sulfur concentrations in the gas phase (H_2S/SiH_4) less than about 10^{-6} the initial efficiencies of the sulfur-containing cells are identical with those of control cells. The stability of these cells, as compared to those of the a-Si:H control cells, are the same within experimental error. For sulfur fractions greater than 10^{-6} the initial efficiencies drop slowly (less than one percent in initial efficiency for fractions less than about 10^{-5}). The degradation of these cells is still measurable, although the final degraded efficiencies are better for the cells with higher sulfur concentrations.

It appears that sulfur provides some improvement in the stabilities if cells with thick i-layers, but we have been unable to produce cells that exhibit no degradation using this approach. Therefore, absent an unanticipated breakthrough, further research in this area is problematic.

8. CONCLUSIONS

The major accomplishments of the three phases of the sub-contract are (1) the development of a second harmonic detection technique for ESR and optically excited ESR (LESR) in a-Si:H and related alloys, (2) the discovery of universal kinetics for the decay of optically excited electrons and holes in a-Si:H and related alloys at low temperatures, (3) the first detection of optically excited band tail electrons and holes in hydrogenated amorphous germanium (a-Ge:H), (4) the first electron spin resonance (ESR) study of the kinetics for the production of silicon dangling bonds in a-Si:H at low temperatures, and (5) the determination from ^{1}H NMR that there exists an order of magnitude more molecular hydrogen (H_2) in a-Si:H than previously measured. In conjunction with our previous results on low-temperature LESR in a-Si:H, the third accomplishment shows that the decay of optically excited band tail electrons and holes at low temperatures is a universal feature of tetrahedrally-coordinated amorphous semiconductors. The determinations of molecular hydrogen concentrations in both PECVD and HWCVD samples show clearly that there are distinct differences between these two types of a-Si:H. In particular, the HWCVD samples with low hydrogen concentrations also have low molecular hydrogen concentrations and possess a more ordered local silicon network. Finally, the low temperature kinetic experiments for the production of silicon dangling bonds in a-Si:H show clearly that the existing models must be modified to account for the slower rates of production at very low temperatures.

The three-chamber, load-locked PECVD deposition system is routinely producing intrinsic and doped films of a-Si:H. In the a-Si:H materials system, we have made cells with moderate efficiencies based on the p-i-n architecture and compared them to cells where the i-layers are sulfur doped. For thick i-layers, the degradations of the sulfur doped cells are less than those of the cells based on intrinsic a-Si:H, but the improvement is not sufficient to warrant further study at present.

9. REFERENCES

1. B. Yan and P. C. Taylor, MRS Symp. Proc. (1998), in press.
2. W. E. Carlos, Naval Research Laboratory, Washington, D. C., private communication.
3. G. Schumm, W. B. Jackson, and R. A. Street, Phys. Rev. **B48**, 14198 (1993).
4. S. C. Deane and M. J. Powell, Phys. Rev. **B48**, 10815 (1993).
5. M. Gunes, C. R. Wronski, and T. J. McMahon, J. Appl. Phys. **76**, 2260 (1994).
6. M. Gunes and C. R. Wronski, J. Appl. Phys. **81**, 3526 (1997).
7. V. Nadady, R. Durny, and E. Pincik, Phys. Rev. Lett. **78**, 1102 (1997).
8. S. L. Wang, J. M. Viner, M. Anani and P. C. Taylor, J. Non-Cryst. Solids **164-166,** 251 (1993).
9. S. Chen and P. C. Taylor, unpublished.
10. D. Caputo, G. De Cesare, F. Palma, M. Tucci, C. Minarini and E. Terzini, Mat. Res. Soc. Symp. **467**, 91 (1997).
11. S. L. Wang and P. C. Taylor, Solid State Commun. **95**, 361 (1995).
12. H. G. Grimmeiss and E. Janzen, in *Deep Centers in Semiconductors,* edited by S. T. Pantelides (Gordon and Breach Science Publisher, New York, 1986), p. 87.
13. S. L. Wang, Z. H. Lin, I M. Viner and P. C. Taylor, Mat. Res. Soc. Symp. Proc. **336**, 559 (1994).
14. B. Yan and P. C. Taylor, Mat. Res. Soc. Symp. Proc. **467**, 103 (1997).
15. D. Redfield and R. H. Bube, Appl. Phys. Lett. **54**, 1037 (1989).
16. N. Hata and S. Wagner, J. Appl. Phys. **72**, 2857 (1992).
17. H. Fritzsche, Mat. Res. Soc. Symp. Proc. **467**, 19 (1997).
18. M. H. Brodsky and R. S. Title, Phys. Rev. Lett. **23**(11), 581 (1969).
19. J. C. Knights, D. K. Biegelsen, and I. Solomon, Solid State Commun. **22**, 133 (1977).
20. R.A. Street and D. K. Biegelsen, Solid State Commun. **33**, 1159 (1980).
21. M. Stutzmann and J. Stuke, Solid State Commun. **47**(8), 635 (1983).

22. J. R. Pawlik and W. Paul, Proc. 7th Int. Conf. on Amorphous and Liquid Semiconductors, 437 (1977).

23. M. H. Brodsky, in Amorphous Semiconductors, Springer-Verlag (1985).

24. G. E. Moore, Natl. Bur. Stand., Cir. No.467 (1949).

25. B. Yan and P.C. Taylor, MRS Symposium Proceeding, **507**, 787 (1998).

26. G. Schumm, W. B. Jackson, and R.A. Street, Phys. Rev. B **48**(19), 14198 (1993).

27. B. Yan, N. Schulz, A. L. Efros, and P. C. Taylor, Phys. Rev. Lett. **84**, 4180 (2000).

28. E. I. Levin, S. Marianer, and B. I. Shklovskii, Phys. Rev. B **45**, 5906 (1992).

29. F. Boulitrop and D. J. Dunstan, Solid State Commun. **44**, 841 (1982).

30. D. L. Staebler and C. R. Wronski, Appl. Phys. Lett. **31**, 292 (1977).

31. P. Stradins and H. Fritzsche, Phil. Mag. **B69**, 121 (1994).

32. P. Stradins and H. Fritzsche, J. Non-Cryst. Solids **198-200**, 432 (1996).

33. H. Branz, Solid State Commun. **105**, 387 (1998).

34. T. Umeda, S. Yamasaki, J. Isoya, A. Matsuda, K. Tanaka, Phys. Rev. Lett. **77**, 4600 (1996).

35. R. A. Street and D. K. Biegelsen, Solid State Commun. **44**, 501 (1982).

36. R. Carius and W. Fuhs, AIP Conf. Proc. **120**, 125 (1984).

37. P. Persans, Phil. Mag. **B46**, 435 (1982).

38. M. Q. Tran, P. Stradins, and H. Fritzsche, MRS Symp. Proc. **336**, 431 (1994).

39. H. Fritzsche, S. Heck, and P. Stradins, J. Non-Cryst. Solids **198-200**, 153 (1996).

40. F. Boulitrop, AIP Conf. Proc. **120**, 178 (1984).

41. M. Stutzmann, W. B. Jackson, and C. C. Tsai, Phys. Rev. **B32**, 23 (1984).

42. R. A. Street and D. K. Biegelsen, Solid State Commun. **44**, 501 (1982).

43. R. Carius and W. Fuhs, AIP Conf. Proc. **120**, 125 (1984).

44. P. Stradins and H. Fritzsche, Phil. Mag. **B69**, 121 (1994).

45. P. Persans, Phil. Mag. **B46**, 435 (1982).

46. M. Q. Tran, P. Stradins, and H. Fritzsche, MRS Symp. Proc. **336**, 431 (1994).

47. H. Fritzsche, S. Heck, and P. Stradins, J. Non-Cryst. Solids **198-200**, 153 (1996).

48. F. Boulitrop, AIP Conf. Proc. **120**, 178 (1984).

49. B. Yan and P. C. Taylor, MRS Symp. Proc. **507**, 805 (1998).

50. See, for example, D. L. Griscom, Phys. Rev. **B20**, 1823 (1979).

51. P. Stradins and H. Fritzsche, MRS Symp. Proc. **467**, 85 (1997).

52. P. Stradins and H. Fritzsche, J. Non-Cryst. Solids **198-200**, 432 (1996).

53. N. A. Schultz and P. C. Taylor, MRS Symp. Proc. **557** (1999) 353.

54. P. C. Taylor, N. A. Schultz, B. Yan, and A. E. Efros, Proceedings of the 25th International Conference on the Physics of Semiconductors, M. Miura and T. Ando, eds. (Springer Verlag, Berlin, 2001), 1477.

55. N. A. Schultz, B. Yan and A. L. Efros), J. Non-Cryst. Solids **266-269** (2000) 372.

56. F. C. Marques , M. M. de Lima, Jr., and P. C. Taylor, Appl. Phys. Lett. **74** (1999) 3797.

57. F. C. Marques, M. M. de Lima, Jr., and P. C. Taylor, J. Non-Cryst. Solids **266-269** (2000) 717.

58. B. I. Shklovskii, H. Fritzsche, and S. D. Baranovskii, Phys. Rev. Lett. **62** (1989) 2989.

59. G. D. Watkins and J. W. Corbett, Phys. Rev. **138** (1965) A543.

60. R. A. Street, D. K. Biegelsen, and R. L. Weisfield, Phys. Rev. B **30** (1984) 5861.

61. T. Umeda, S. Yamasaki, J. Isoya, A. Matsuda, and K. Tanaka, Phys. Rev. Lett. **77** (1996) 4600.

62. P. A. Fedders, D. A. Drabold, and S. Nakhmanson, Phys. Rev. B **58** (1998) 15624.

63. W. E. Carlos and P. C. Taylor, Phys. Rev. B **25**, 1435 (1982); Phys. Rev. B26, 3605 (1982).

64. J. A. Reimer, R. W. Vaughan and J. Knights, Phys. Rev. Lett. **44**, 193 (1980).

65. J. A. Reimer, R. W. Vaughan and J. Knights, Phys. Rev. B **24**, 3360 (1981).

66. J. B. Boyce, and M. Stutzmann, Phys. Rev. Lett. **54**, 562 (1985).

67. F. Reif and E. M. Purcell, Phys. Rev. **91**, 631 (1953).

68. I. F. Silvera, Rev. Mod. Phys. **52**, 393 (1980).

69. X. Liu, B. E. White, Jr., and R. O. Pohl, Phys. Rev. Lett. **78**, 4418 (1997).

70. J. Jeener and P. Broekaert, Phys. Rev. **157**, 232 (1967).

71. P. H. Chan, Ph.D. Thesis, Washington University, September, 1993 (unpublished).

72. P. A. Fedders, R. Fisch, and R. E. Norberg, Phys. Rev. B **31**, 6887 (1985).

73. R. E. Norberg, D. J. Leopold, P. A. Fedders, J. Non-Cryst. Solids, **227-230**, 124 (1998).

74. J. T. Stephen, D. Han, A. H. Mahan, and Y. Wu, Mat. Res. Soc. Symp. Proc. **420**, 485 (1996).

75. T. Su, S. Chen, P. C. Taylor, R. S. Crandall, and A. H. Mahan, Phys. Rev. **B62**, 12849 (2000).

76. M. S. Conradi and R. E. Norberg, Phys. Rev. **B24**, 3360 (1981).

77. G. R. Khutsishvili, Usp. Fiz. Nauk **87**, 211 (1965) [Sov. Phys. Usp. **8**, 743 (1966).

78. P. A. Fedders, Phys. Rev. **B32**, 2739 (1985).

79. A. Abragam, *The Principles of Nuclear Magnetism* (Oxford University Press, London, 1961), p. 378.

80. J. T. Stephen, D. Han, A. H. Mahan, and Y. Wu, in *Amorphous Silicon Technology - 1996*, edited by Michael Hack et al., MRS Symposium Proceedings No. 420 (Materials Research Society, Pittsburgh, 1996), p. 485.

81. P. Hari, P. C. Taylor, and R. A. Street, in *Amorphous Silicon Technology-1994*, edited by E. A. Schiff et al., MRS Symp. Proc. No. 336 (Materials Research Society, Pittsburgh, 1994), p. 293

82. P. Hari, P. C. Taylor, and R. A. Street, in *Amorphous Silicon Technology-1995*, edited by M. Hack et al., MRS Symp. Proc. No. 377 (Materials Research Society, Pittsburgh, 1995), p. 185.

83. P. H. Chan, Ph.D. thesis, Washington University, 1993.

84. D. Tse and S. R. Hartmann, Phys. Rev. Lett. **21**, 511 (1968).

85. I. J. Lowe and D. Tse, Phys. Rev. **166**, 279 (1968).

86. H. -J. Stöckmann and P. Heitjans, J. Non-Cryst. Solids **66**, 501 (1984).

87. H. T. Stokes and D. A. Ailion, Phys. Rev. **B16**, 4746 (12977).

88. J. Jeener, H. Eisendrath, and R. Van Steenwinkel, Phys. Rev. **133**, A478 (1964).

89. P. Broekaert and J. Jeener, Phys. Rev. **B15**, 4168 (1977).

90. M. Stutzmann and D. K. Biegelsen, Phys. Rev. **B28**, 6256 (1983).

91. M. Stutzmann and D. K. Biegelsen, Phys. Rev. **B34**, 3093 (1986).

10. PUBLICATIONS

1. "Relaxation to Hopping Conductivity in Sulfur-Doped Hydrogenated Amorphous Silicon" (J.-H. Yoon and P. C. Taylor), J. Non-Cryst. Solids **227-230**, 385 (1998).

2. "Light-Induced Recombination Centers in Hydrogenated Amorphous Silicon-Sulfur Alloys" (J.-H. Yoon, P. C. Taylor, and Czang-Ho Lee), J. Non-Cryst. Solids **227-230**, 324 (1998).

3. "Effect of Sulfur Doping on electrical Conductivity of a-Si:H" (R. M. Mehra, Jasmina, P. C. Mathur, and P. C. Taylor), Thin Solid Films **312**, 170 (1998).

4. "Kinetics of Light Induced Defect Formation and Annealing in Hydrogenated Amorphous Silicon Alloyed with Sulfur" (B. Yan, S. L. Chen, and P. C. Taylor), MRS Symp. Proc. **507**, 453 (1998).

5. "Study of Photoconductivity and Persistent Photoconductivity in Sulphur-doped Amorphous Hydrogenated Silicon" (R. M. Mehra, Jasmina, P. C. Mathur, and P. C. Taylor), Int. J. Electronics **86**, 1321 (1999).

6. "Properties of Hydrogenated Amorphous Silicon Films Alloyed with Selenium" (S. L. Chen, J. M. Viner, and P. C. Taylor), MRS Symp. Proc. **507**, 459 (1998).

7. "Optical Properties of Large Band Gap Se- and S-doped Amorphous Hydrogenated Silicon" (R. M. Mehra, J. Baveja, L. P. Purohit, R. Jumar, A. V. Singh, P. C.. Mathur, and P. C. Taylor), J. Non-Cryst. Solids **266-269**, 708 (2000).

8. "Photoluminescence in Hydrogenated Amorphous Silicon Alloyed with Selenium", W. Xu, S. L. Chen, and P. C. Taylor, Homage Book - Andrei Andriesh (INOE&INFM Publishing House, Bucharest, 1999), M. Popescu, ed., p. 45-52; also Rom. Rpts. in Phys. **51**, 1 (2000).

9. "Study of Photoconductivity in TBP Doped n-Type Hydrogenated Amorphous Silicon Using Argon as Carrier Gas" (R. M. Mehra, I. Kaur, P. C. Mathur, and P. C. Taylor), J. Non-Cryst. Solids **227-230**, 243 (1998).

10. "Comparison of Theoretical Models with Experimental Data of the Midgap States in Undoped Hydrogenated Amorphous Silicon", G. Mensing, J. M. Gilligan, P. Hari, N. H. Tolk, and P. C. Taylor, J. Non-Cryst. Solids (2002), in press.

11. "Defect Structure in Nitrogen-Rich Amorphous Silicon Nitride Films" (B. Yan, J. H. Dias da Silva, and P. C. Taylor), J. Non-Cryst. Solids **227-230**, 528 (1998).

12. "Localized Electronic States in a-Si:H as Determined from ESR and LESR" (P. C. Taylor), in *Properties of Amorphous Silicon and its Alloys*, T. Searle, ed. (INSPEC, London, 1998), p. 139.

13. “Excitation Intensity Dependence of Light-Induced Electron Spin Resonance in Hydrogenated Amorphous Silicon Films” (B. Yan and P. C. Taylor), MRS Symp. Proc. **507**, 787 (1998).

14. “Excitation Energy Dependence of Photoinduced Absorption in Intrinsic a-Si:H” (N. Schultz, Z. V. Vardeny, and P. C. Taylor), MRS Symp. Proc. **507**, 745 (1998).

15. “Universal Distribution of Residual Carriers in Tetrahedrally-Coordinated Amorphous Semiconductors”, B. Yan, N. Schultz, A. L. Efros, and P. C. Taylor, Phys. Rev. Lett. **84**, 4180 (2000).

16. “Low Temperature Kinetics for the Growth and Decay of Band-tail Carriers and Dangling Bonds in Hydrogenated Amorphous Silicon”, N. Schultz and P. C. Taylor, MRS Symp. Proc. **557**, 353 (1999).

17. “Recombination Kinetics of Long-Lived Carriers in a-Si:H at Low Temperatures”, N. Schultz, B. Yan, A. L. Efros, and P. C. Taylor, J. Non-Cryst. Solids **266-269**, 372 (2000).

18. “Universal Distribution of Optically Excited Carriers in Tetrahedral Amorphous Semiconductors” (N. A. Schultz, B. Yan, A. L. Efros, and P. C. Taylor), Proceedings of the 25th International Conference on the Physics of Semiconductors, M. Miura and T. Ando, eds. (Springer Verlag, Berlin, 2001), 1477.

19. “Light-Induced Electron Spin Resonance in Amorphous Hydrogenated Germanium”, F. C. Marques, M. M de Lima, Jr., and P. C. Taylor, Appl. Phys. Lett. **74**, 3797 (1999).

20. “Optically Excited Paramagnetic Centers in Amorphous Hydrogenated Germanium”, F. C. Marques, M. M. de Lima, Jr., and P. C. Taylor, J. Non-Cryst. Solids **266-269**, 717 (2000).

21. “Low Temperature, Light Induced Production of Silicon Dangling Bonds in Hydrogenated Amorphous Silicon”, N. A. Schultz and P. C. Taylor, Phys Rev. B (2001), submitted.

22. “NMR Study of Ortho-Molecular Hydrogen in Hydrogenated Amorphous Silicon”, T. Su, S. L. Chen, P. C. Taylor, R. S. Crandall, and A. H. Mahan, MRS Symp. Proc. **557**, 293 (1999).

23. “Ortho-molecular Hydrogen in Hydrogenated Amorphous Silicon”, T. Su, P. C. Taylor, R. S. Crandall, and A. H. Mahan), Appl. Phys. Lett. **76**, 565 (2000).

24. “Molecular Hydrogen in Amorphous Silicon Revisited”, T. Su, S. L. Chen, P. C. Taylor, R. S. Crandall, and A. H. Mahan, J. Non-Cryst. Solids **266-269**, 195 (2000).

25. “Molecular Hydrogen in Hydrogenated Amorphous Silicon: New Evidence from NMR”, T. Su, S. Chen, P. C. Taylor, R. S. Crandall, and A. H. Mahan, Phys. Rev. B **62**, 12849 (2000).

26. “Observation of Fine Structure in the Photoluminescence Spectrum of an Er^{3+} Ion in an Amorphous Silicon Matrix” (A. A. Andreev, V. G. Golubev, A. V. Medvedev, A. B. Pevtsov, N. A. Feoktistov, V. F. Masterov, S. B. Aldabergenova, and P. C. Taylor), JETP Letters **70**, 797 (1999).

27. “Microscopic Origin of Er^{3+} Emission in Mixed Amorphous-Nanocrystalline Si:H Films” (S. B. Aldabergenova, P. C. Taylor, M. Albrecht, H. P. Strunk, J. Viner, and A. A. Andreev) Mat. Sci. and Eng. **B81**, 29 (2001).

28. “AFM and Raman Studies of Grain Sizes in Microcryatalline SI:H” (C. Inglefield, P. C. Taylor, and A. Madan) MRS Symp. Proc. (2001), in press.

29. “Photovoltaic Applications of Amorphous Silicon: The Journey from Basic Research to Development,” (P. C. Taylor), Egypt. J. Sol. **21**, 291 (1998).

REPORT DOCUMENTATION PAGE

Form Approved
OMB NO. 0704-0188

Public reporting burden for this collection of information is estimated to average 1 hour per response, including the time for reviewing instructions, searching existing data sources, gathering and maintaining the data needed, and completing and reviewing the collection of information. Send comments regarding this burden estimate or any other aspect of this collection of information, including suggestions for reducing this burden, to Washington Headquarters Services, Directorate for Information Operations and Reports, 1215 Jefferson Davis Highway, Suite 1204, Arlington, VA 22202-4302, and to the Office of Management and Budget, Paperwork Reduction Project (0704-0188), Washington, DC 20503.

1. AGENCY USE ONLY (Leave blank)	2. REPORT DATE	3. REPORT TYPE AND DATES COVERED
	March 2002	Final Technical Report January 1998 – October 2001

4. TITLE AND SUBTITLE
Characterization of Amorphous Silicon Thin Films and PV Devices,
Final Technical Report, January 1998 – October 2001

5. FUNDING NUMBERS
CF: XAK-8-17619-13
PVP25001

6. AUTHOR(S)
P.C. Taylor

7. PERFORMING ORGANIZATION NAME(S) AND ADDRESS(ES)
University of Utah
Salt Lake City, Utah

8. PERFORMING ORGANIZATION REPORT NUMBER

9. SPONSORING/MONITORING AGENCY NAME(S) AND ADDRESS(ES)
National Renewable Energy Laboratory
1617 Cole Blvd.
Golden, CO 80401-3393

10. SPONSORING/MONITORING AGENCY REPORT NUMBER
NREL/SR-520-31984

11. SUPPLEMENTARY NOTES
NREL Technical Monitor: Bolko von Roedern

12a. DISTRIBUTION/AVAILABILITY STATEMENT
National Technical Information Service
U.S. Department of Commerce
5285 Port Royal Road
Springfield, VA 22161

12b. DISTRIBUTION CODE

13. ABSTRACT *(Maximum 200 words)* This report describes the most significant results of the three phases: (1) development of a second harmonic detection technique for electron spin resonance (ESR) and optically excited ESR (LESR) in a-Si:H and related alloys, (2) discovery of universal kinetics for the decay of optically excited electrons and holes in a-Si:H and related alloys at low temperatures, (3) first detection of optically excited band-tail electrons and holes in hydrogenated amorphous germanium (a-Ge:H), (4) first ESR study of the kinetics for the production of silicon dangling bonds in a-Si:H at low temperatures, and (5) determination from ^{1}H NMR that there exists an order of magnitude more molecular hydrogen (H_2) in a-Si:H than previously measured.

14. SUBJECT TERMS: PV; hydrogenated amorphous silicon; microcrystalline alloys; thermal deflection spectroscopy (PDS); photoluminescence; electron spin resonance (ESR); constant photocurrent method; nuclear magnetic resonance (NMR)

15. NUMBER OF PAGES

16. PRICE CODE

17. SECURITY CLASSIFICATION OF REPORT	18. SECURITY CLASSIFICATION OF THIS PAGE	19. SECURITY CLASSIFICATION OF ABSTRACT	20. LIMITATION OF ABSTRACT
Unclassified	Unclassified	Unclassified	UL

NSN 7540-01-280-5500

Standard Form 298 (Rev. 2-89)
Prescribed by ANSI Std. Z39-18
298-102